Rapid reconnection in compressible plasma

Martin F. Heyn[a)]
Institut für Theoretische Physik, Technische Universität Graz, Petersgasse 16, A-8010 Graz, Austria

Vladimir S. Semenov
Institute of Physics, State University St. Petersburg, St. Petergof 198904, Russia

(Received 4 January 1996; accepted 4 April 1996)

A study of set-up, propagation, and interaction of non-linear and linear magnetohydrodynamic waves driven by magnetic reconnection is presented. The source term of the waves generated by magnetic reconnection is obtained explicitly in terms of the initial background conditions and the local reconnection electric field. The non-linear solution of the problem found earlier, serves as a basis for formulation and extensive investigation of the corresponding linear initial-boundary value problem of compressible magnetohydrodynamics. In plane geometry, the Green's function of the problem is obtained and its properties are discussed. For the numerical evaluation it turns out that a specific choice of the integration contour in the complex plane of phase velocities is much more effective than the convolution with the real Green's function. Many complex effects like intrinsic wave coupling, anisotropic propagation characteristics, generation of surface and side wave modes in a finite beta plasma are retained in this analysis. © *1996 American Institute of Physics.* [S1070-664X(96)02907-2]

I. INTRODUCTION

Magnetic reconnection is a pictorial description of a fairly complex process occurring in highly conducting magnetized fluids. The key point is that magnetic field lines are 'cut and reconnected', i.e., the field topology is changed locally. This has far reaching consequences, e.g., energy stored in large-scale magnetic field configurations is released in a rapid manner (solar flares), planetary magnetic flux tubes are 'opened' to the interplanetary magnetic field leading to efficient coupling of solar wind momentum into the magnetosphere via magnetic stresses (magnetopause reconnection), and major disruptions are caused by magnetic reconnection in plasma confinement devices such as a tokamak.

A basic prerequisite for the occurrence of magnetic reconnection is the capability of a highly conducting plasma to form very thin current layers. Current layers have been detected in highly conducting fluids with and without collisions. An excellent example for a collisionless current layer is the dayside magnetopause which is formed by large-scale magneto-convection of solar wind plasma against the Earth's intrinsic magnetic field. Current layers have been also observed in many other sites, e.g., near other planets, in the solar photo-sphere, in inter-stellar space, in laboratory plasma devices, etc.

Particle models of collisionless current layers have first been formulated and solved in the 1950s.[1–4] In a collisionless plasma, the thickness of current layers is of the order of an ion gyro-radius which is often orders of magnitudes less than other global length scales, e.g., the radius of curvature of the magnetopause. Therefore, in situations with spatial scales much larger than the ion gyro-radius, the current layer may as well be approximated by a current carrying surface.

In magnetohydrodynamic (MHD) theory, the width of an equivalent current sheath would be proportional to $1/\sigma^{\alpha}$, where σ is some effective conductivity of the fluid with some exponent α. In the ideal limit, the plasma conductivity σ goes to infinity and the sheath shrinks to a sheet, the infinite current density being then better defined by some (finite) surface current density. Across such a surface, the magnetohydrodynamic quantities like velocity, magnetic field, density, and pressure will, in general, suffer a jump. The occurrence of magnetic reconnection is bound up with a particular discontinuity of such type, namely a tangential discontinuity carrying magnetic shear.

The first models[5,6] to explain the release of magnetic energy through the formation of current layers were based on pure magnetic field diffusion (field annihilation models). As a consequence, the characteristic time scales obtained are very slow because diffusion is needed over large spatial scales and the corresponding magnetic Reynolds numbers are extremely high. On the other hand, for magnetic reconnection to occur it is sufficient to have a local enhancement of the electrical resistivity in an otherwise highly conducting fluid. Consequently, the assumption of an ideal conducting plasma which does not allow for a 'slipping' of the magnetic field lines with respect to the flow should be dropped in this local region. But from the point of view that this generic process is extremely localized, the reconnection region can also be understood as a pure source of MHD waves which transport the information into a wider region where the assumption of an ideal plasma still holds.[7–9]

From the view point of ideal MHD theory, magnetic reconnection causes the non-linear decay of an infinitely thin current sheet, i.e., a tangential discontinuity, into large amplitude MHD waves.[10] This can be understood by the appearance of a localized electric field E^* along some reconnection line in the plane of the tangential discontinuity. If this electric field is small compared to the electric field based on Alfvén velocity and background magnetic field $E_A = v_A B/c$, a perturbation expansion in the small parameter E^*/E_A is appropriate. The tangential discontinuity develops

a) Electronic mail: heyn@itp.tu-graz.ac.at

Downloaded¬09¬Apr¬2003¬to¬193.170.90.47.¬Redistribution¬subject¬to¬AIP¬license¬or¬copyright,¬see¬http://ojps.aip.org/pop/popcr.jsp

into a structured boundary layer because the electric field E^* is transported away from the reconnection site with approximately the Alfvén speed.

The whole problem naturally splits into a non-linear part, i.e., the decay of a tangential discontinuity into a boundary layer formed by large-amplitude waves (Riemannian problem) and a linear free-boundary MHD problem where shape and speed of the large amplitude waves have to be determined in a self-consistent way with the neighboring linear perturbations of plasma flow and magnetic field. The solution of the non-linear part is now well known,[11–14] whereas the linear part, up to now, has been studied primarily either in the (incompressible and compressible) steady state limit[15–18] or the time dependent incompressible limit.[19–23] Results on the structure of reconnection layers and incompressible spontaneous reconnection are reviewed in Refs. 24, 25.

Computer studies on fast reconnection for different resistivity models and external boundary conditions have been published recently.[26–28] The results of these numerical studies are in agreement with the results of the present study.

In comparison to rapid reconnection, magnetic reconnection has also been studied in form of tearing mode instabilities[29] and its non-linear extensions.[30] Although this mechanism works faster than pure field dissipation it is a process where the plasma flow and magnetic field reconfiguration has a localized nature.

In the present paper, a fairly complete description of time dependent magnetic reconnection in a compressible plasma is given. The linear analysis of this problem, to a large extent, resembles the study of the Kelvin–Helmholtz instability of a discontinuity surface in a compressible plasma. Magnetic field reconnection widens this ideal surface into a boundary layer with internal structure, essentially defined by the reconnection electric field, stress, and pressure balance.

The governing equations of ideal MHD, the conservation laws across MHD discontinuities and the equations for one-dimensional large amplitude simple MHD waves, together with some general consequences for reconnection are summarized in Section II. The basic results for the non-linear part of the analysis (Riemannian problem) are stated in Section III. In Section IV, the appropriate linearized equations in Fourier space are derived. Then, from the pressure balance condition, the solution for the perturbations in the inflow regions is obtained. The study of the evolution of normal magnetic field and velocity within the boundary layer will give the connection for the solution in the upper and the lower half spaces in terms of the reconnection electric field.

In Section V, a method originally introduced in Ref. 31, is worked out that allows for the inversion from Fourier to real space of the exact linearized MHD system in plane geometry with different homogeneous background states in the upper and lower half planes. The solutions for each half plane are coupled by pressure balance in zero and first order along the interface axis. With this powerful method, the Green's function (propagator) of the system is obtained explicitly. The general solution can be expressed as a folding of the reconnection electric field with this Green's function. In the case of reconnection, the sources which induce the perturbations in the half planes are moving with super and subsonic speeds along the interface axis. The solution describes the self-consistent temporal evolution of shape and strength of the different shock waves and discontinuities traveling along the current layer as well as the perturbations in the adjacent half planes generated by the prescribed electric field along the given reconnection line.

In addition this technique can also be used to study the evolution of compressible magnetohydrodynamic perturbations in two half planes with different wave properties. Perturbation sources, moving or not, can be distributed arbitrarily in each half plane. The effects of compressibility, anisotropic wave propagation, and coupling of waves (intrinsic and via pressure balance condition) are all taken into account without any further approximation.

II. BASIC EQUATIONS

The governing equations, expressing the conservation of mass, momentum, energy, and magnetic flux for an ideal, infinitely conducting, magnetized fluid in conservation form are

$$\frac{\partial \rho}{\partial t} + \operatorname{div}(\rho \mathbf{v}) = 0, \tag{1a}$$

$$\frac{\partial (\rho \mathbf{v})}{\partial t} + \operatorname{div}\left[\rho \mathbf{v}\mathbf{v} + p\mathbf{I} - \frac{1}{4\pi}\left(\mathbf{B}\mathbf{B} - \frac{B^2}{2}\mathbf{I}\right)\right] = 0, \tag{1b}$$

$$\frac{\partial}{\partial t}\left(\frac{1}{2}\rho v^2 + \rho e + \frac{B^2}{8\pi}\right) + \operatorname{div}\left[\rho \mathbf{v}\left(\frac{v^2}{2} + e + \frac{p}{\rho}\right) + \frac{1}{4\pi}\mathbf{B}\times(\mathbf{v}\times\mathbf{B})\right] = 0, \tag{1c}$$

$$\frac{\partial \mathbf{B}}{\partial t} + \operatorname{div}(\mathbf{B}\mathbf{v} - \mathbf{v}\mathbf{B}) = 0. \tag{1d}$$

Here, ρ is the mass density, $\mathbf{v}$ the fluid velocity, $\mathbf{B}$ the magnetic field, p the isotropic fluid pressure, $e = [1/(\gamma - 1)]p/\rho$ the internal energy, and $\mathbf{I}$ the unit dyadic. The electric field $\mathbf{E}$ is related to velocity and magnetic field by $\mathbf{E} = -(1/c)\mathbf{v}\times\mathbf{B}$.

A. MHD discontinuities

In addition to continuous solutions, this hyperbolic set of equations also allows for generalized solutions including discontinuities, if the following conditions across the surface of discontinuity are satisfied:[32]

$$[\![m]\!] = 0, \tag{2a}$$

$$\left[\!\!\left[m\mathbf{v} + \mathbf{n}\left(p + \frac{B^2}{8\pi}\right) - \frac{B_n}{4\pi}\mathbf{B}\right]\!\!\right] = 0, \tag{2b}$$

$$\left[\!\!\left[m\left(\frac{v^2}{2} + e + \frac{B^2}{8\pi\rho}\right) + v_n\left(p + \frac{B^2}{8\pi}\right) - \frac{B_n}{4\pi}\mathbf{v}\cdot\mathbf{B}\right]\!\!\right] = 0, \tag{2c}$$

$$[\![(v_n - u)\mathbf{B} - B_n\mathbf{v}]\!] = 0, \tag{2d}$$

$$[\![B_n]\!] = 0, \tag{2e}$$

Downloaded¬09¬Apr¬2003¬to¬193.170.90.47.¬Redistribution¬subject¬to¬AIP¬license¬or¬copyright,¬see¬http://ojps.aip.org/pop/popcr.jsp

where $m \equiv \rho(v_n - u)$ is the mass flux through the discontinuity and square brackets $[\![\ ]\!]$ denote the difference of the quantities across the moving discontinuity surface with unit normal $\mathbf{n}$ and speed u.

This system of conservation laws is equivalent to the following equation[33]

$$m\left(m^2\langle\tau\rangle - \frac{B_n^2}{4\pi}\right)\left\{m^4\langle\tau\rangle - m^2\left(\frac{1}{4\pi}\langle\mathbf{B}\rangle^2 - \langle\tau\rangle\frac{[\![p]\!]}{[\![\tau]\!]}\right) - \frac{B_n^2}{4\pi}\frac{[\![p]\!]}{[\![\tau]\!]}\right\} = 0, \tag{3}$$

and the equation

$$[\![\mathbf{v}]\!]^2 = m^2[\![\tau]\!]^2 + \frac{1}{4\pi}[\![\tau\mathbf{B}]\!]\cdot[\![\mathbf{B}]\!], \tag{4}$$

which relates the change in speed to the change in normal dynamic pressure and to the change in magnetic field and density. Here, $\tau \equiv 1/\rho$ denotes the specific volume and the bracket $\langle\rangle$ is the average of conditions on the two sides of the discontinuity.

The root $m = 0$ of (3) is associated with a tangential discontinuity, $[\![p + B^2/(8\pi)]\!] = 0$, or, if $B_n \neq 0$, with a contact discontinuity, $[\![p]\!] = [\![\mathbf{B}]\!] = [\![\mathbf{v}]\!] = 0$.

The root $m^2\langle\tau\rangle - B_n^2/(4\pi) = 0$ of (3) is associated with an Alfvén discontinuity or rotational discontinuity, $[\![\tau]\!] = [\![e]\!] = [\![p]\!] = [\![u_n]\!] = [\![\mathbf{B}^2]\!] = 0$. These are the only MHD discontinuities which do not modify the thermodynamic properties of the fluid and allows for an arbitrary rotation of the magnetic field across the surface of the discontinuity.

The roots of the fourth-degree polynomial in m of the expression inside the curly brackets in (3), $m^4\langle\tau\rangle - m^2(\langle\mathbf{B}\rangle^2/(4\pi) - \langle\tau\rangle[\![p]\!]/[\![\tau]\!]) - B_n^2[\![p]\!]/(4\pi[\![\tau]\!]) = 0$, are referred to as fast or slow (compressive) shocks; they are large amplitude versions of the fast and slow MHD modes respectively.

Across a tangential discontinuity, there is neither mass nor magnetic flux (velocity and magnetic fields are tangential), and the total pressure $p + B^2/(8\pi)$ is continuous. This is a marginal stable situation, because there is free energy in the system in the form of tangential stresses stored in the (arbitrary) shear of plasma flow and magnetic field. Any local breakdown of the perfect conductivity approximation will entail a sudden reconfiguration of the system. The magnetic field can diffuse and the resulting magnetic flux through the surface (magnetic field lines are 'cut and reconnected') sets free the energy stored in the unbalanced tangential stresses. The surface gets non-linearly unstable, i.e., within the time scale needed for wave steepening, non-linear (large-amplitude) MHD shear and entropy waves will be formed in order to balance the tangential stresses. The wave steepening time depends on the gradient in the initial profile of the relevant quantities (pressure, density, etc.). In the idealized case of a discontinuous initial profile such as a tangential discontinuity, steepening occurs instantaneously.

The situation is similar to the Mach reflection problem after collision of two shock waves. When shock waves collide, an unstable surface is formed. In order to balance energy, momentum and mass fluxes, a set of different large-amplitude waves will emerge from it in the form of transmitted and reflected waves. The number of waves corresponds to the number of degrees of freedom of the problem at hand. In gas dynamics, a typical situation of this type is realized in a shock tube. In this case an unstable surface is set up by breaking the diaphragm separating two regions of different density and pressure. As a result, a shock wave, a rarefaction wave (in this case in form of a centered expansion fan) and a contact discontinuity will emerge which are non-linear versions of the linear sound and entropy waves. Any unbalanced pressure gradients will drive sound waves, whereas any unbalanced density gradients will drive entropy waves. For zero viscosity, the fluid cannot support shear waves. Any unbalanced shear in the flow will excite unstable surface modes (Kelvin–Helmholtz instability).

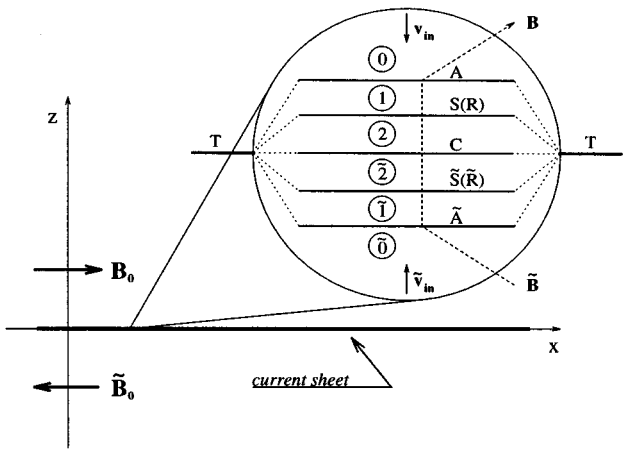

FIG. 1. The current sheet in form of a tangential discontinuity T at $z = 0$ separates two uniform but different plasma and field regions (subscript 0) initially. Reconnection at the reconnection line (the y axis) produces a normal magnetic field component which is transported away from the reconnection site by MHD waves. This normal magnetic field component causes the decay of the current sheet into a set of moving large-amplitude MHD waves (Riemannian problem). As a result, a structured boundary layer object at $z = 0$ is formed with finite plasma flow and magnetic flux through its boundaries.

In magnetohydrodynamics, due to the presence of a magnetic field, shear stresses can be transported throughout the fluid even in the absence of finite viscosity or resistivity. The waves supporting shear are the Alfvén wave and a new branch of sound wave, the slow wave. Because of total pressure balance across a tangential discontinuity, the fast wave which corresponds to the hydrodynamic sound wave will not be driven strongly when such a discontinuity gets unstable through reconnection.

But the tangential discontinuity will instantaneously decay into a set of large-amplitude Alfvén (A) waves, slow shock (S) or rarefaction (R) waves separated by a contact (C) discontinuity in the center as shown in Figure 1. This is the first task to be solved. In more mathematical terms it is stated as looking for one-dimensional time dependent solutions of the ideal MHD system. This system forms a quasi-linear symmetric hyperbolic system of partial differential equations. Characteristic surfaces and Riemann invariants are well defined and the MHD decay problem is therefore also known as 'generalized' Riemannian problem.

Downloaded¬09¬Apr¬2003¬to¬193.170.90.47.¬Redistribution¬subject¬to¬AIP¬license¬or¬copyright,¬see¬http://ojps.aip.org/pop/popcr.jsp

This non-linear decay mode of a tangential discontinuity is of particular importance in the context of reconnection. A small normal magnetic field component B_n introduced in a localized region of the tangential (T) discontinuity (diffusion region), will cause the decay of T into shock waves and discontinuities where the number of waves exactly corresponds to the number of free parameters in the problem: tangential components of magnetic field and velocity, density and pressure subject to total pressure balance. The jumps of these quantities are in lowest order with respect to the ratio $B_n/|\mathbf{B}_t|$ independent of the amplitude of B_n and can be calculated like the one-dimensional Riemannian problem with the normal dynamic pressure neglected.

The fast waves which have been neglected so far, are of small amplitude but nevertheless important because they will generate the appropriate inward flow in the external regions necessary for reconnection. These perturbations of flow and magnetic field have to be determined from the MHD equations, linearized with respect to the non-linear solution described above, in a self-consistent way together with the shape of the discontinuities.

B. Simple waves

Large amplitude continuous solutions of system (1a)-(1d) can be obtained, if all MHD quantities are assumed to depend on t and $\mathbf{x}$ in terms of a common function only, say $\varphi(t,\mathbf{x})$. Let a moving surface with unit normal $\mathbf{n}$ and speed u be defined by $\varphi(t,\mathbf{x})=0$, so that

$$u=-\frac{\partial\varphi/\partial t}{|\nabla\varphi|},\quad \mathbf{n}=\frac{\nabla\varphi}{|\nabla\varphi|}, \tag{5}$$

and therefore,

$$\left(\frac{\partial}{\partial t}+\mathbf{v}\cdot\nabla\right)\varphi=(v_n-u)|\nabla\varphi|.$$

Then the MHD equations with $c\equiv v_n-u$ read,[34]

$$c\,\mathrm{d}\rho+\rho\,\mathrm{d}v_n=0, \tag{6a}$$

$$\rho c\,\mathrm{d}\mathbf{v}_t-\frac{B_n}{4\pi}\mathrm{d}\mathbf{B}_t=0, \tag{6b}$$

$$\rho c\,\mathrm{d}v_n+c_s^2\mathrm{d}\rho+\frac{1}{4\pi}\mathbf{B}\cdot\,\mathrm{d}\mathbf{B}_t=0, \tag{6c}$$

$$c\,\mathrm{d}\mathbf{B}-B_n\mathrm{d}\mathbf{v}+\mathbf{B}\mathrm{d}v_n=0, \tag{6d}$$

$$c\,\mathrm{d}S=0, \tag{6e}$$

where the indices n and t refer to projections normal and tangential to the surface defined by $\varphi(t,\mathbf{x})=0$ and S is the entropy by unit mass.

The condition of a zero coefficient determinant for this homogeneous set of equations for $\mathrm{d}\rho$, $\mathrm{d}\mathbf{v}_t$, $\mathrm{d}v_n$, $\mathrm{d}\mathbf{B}_t$, $\mathrm{d}B_n$, $\mathrm{d}S$ gives the speeds of large-amplitude entropy waves, $c=0$, large amplitude Alfvén waves, $c_a=v_{An}$, and large-amplitude fast and slow waves,

$$c_\pm=\left\{\frac{1}{2}[(v_A^2+c_s^2)\pm\sqrt{(v_A^2+c_s^2)^2-4c_s^2v_{An}^2}]\right\}^{1/2}. \tag{7}$$

Here, $\mathbf{v}_A=\mathbf{B}/\sqrt{4\pi\rho}$ is the Alfvén velocity and $c_s=\sqrt{\gamma p/\rho}$ is the sound speed. In the limit $v_{An}\ll v_A^2+c_s^2$ the fast and the slow wave speeds $c_\pm$ approach the limit of quasi-perpendicular wave propagation

$$c_+=\sqrt{v_A^2+c_s^2},\quad c_-=\frac{c_sv_{An}}{\sqrt{v_A^2+c_s^2}}.$$

These results also hold for the phase velocities ω/k of the small amplitude waves of the linearized MHD system. The anisotropic nature of wave propagation can be nicely seen in diagrams of wave normal surfaces (e.g., Ref. 33). The fast wave c_+ propagates in all directions, whereas the Alfvén c_a and the slow c_- wave do not propagate perpendicular to the magnetic field.

III. NON-LINEAR ANALYSIS

In Refs. 12, 13, 20 it is shown how to solve the non-linear decay of a tangential discontinuity into Alfvén discontinuities, slow shocks (rarefaction waves) and a contact discontinuity (see Figure 1).

The upstream quantities (subscript 0) of density, pressure, and the tangential components of $\mathbf{B}$ and $\mathbf{v}$ are related to the downstream values (subscript 1) across an Alfvén discontinuity A by

$$\mathbf{B}_1=\mathbf{b}_1B_0, \tag{8a}$$

$$\mathbf{v}_1=\mathbf{v}_0+\,\mathrm{sgn}(mB_n)(\mathbf{b}_1v_{A0}-\mathbf{v}_{A0}), \tag{8b}$$

$$\rho_1=\rho_0, \tag{8c}$$

$$p_1=p_0, \tag{8d}$$

where $\mathbf{b}_1$ is the still unknown unit vector along the downstream magnetic field (Alfvén parameter). Adding downstream of the Alfvén discontinuity a slow shock S or a rarefaction wave R and neglecting normal flow pressure ($v_n^2\ll v_A^2+c_s^2$), which is reasonable if the decay of a tangential discontinuity is considered, the downstream values (subscript 2) can be parameterized by the change in magnetic field strength, say η, as

$$\mathbf{B}_2=\mathbf{b}_1\,\eta B_0, \tag{9a}$$

$$\mathbf{v}_2=\mathbf{v}_0-\,\mathrm{sgn}(mB_n)[\mathbf{v}_{A0}-\mathbf{b}_1v_{A0}G(\eta)], \tag{9b}$$

$$\frac{\rho_2}{\rho_0}=\begin{cases}1+\dfrac{1-\eta^2}{2\beta+(\gamma-1)(1-\eta)} & (S),\\ \left(\dfrac{p_2}{p_0}\right)^{1/\gamma} & (R),\end{cases} \tag{9c}$$

$$p_2=p_0+\frac{B_0^2}{8\pi}(1-\eta^2), \tag{9d}$$

where

$$G(\eta)=\begin{cases}1-\sqrt{(1-\eta)\left(1-\dfrac{\rho_1}{\rho_2}\eta\right)} & (S),\\ 1+\displaystyle\int_1^\eta \mathrm{d}\eta'\sqrt{\frac{\rho_1}{\rho(\eta')}}\sqrt{1+\frac{v_A^2(\eta')}{c_s^2(\eta')}} & (R).\end{cases}$$

Downloaded¬09¬Apr¬2003¬to¬193.170.90.47.¬Redistribution¬subject¬to¬AIP¬license¬or¬copyright,¬see¬http://ojps.aip.org/pop/popcr.jsp

Here, $\beta \equiv c_s^2/v_{A0}^2$ is closely related to the usual plasma beta (gas pressure over magnetic pressure), and η, as defined in (9a), is the still unknown value for the change in the magnetic field amplitude across slow shock or rarefaction wave (slow wave parameter). Across a slow shock the magnetic field amplitude decreases, $\eta<1$, whereas within a slow rarefaction wave the amplitude increases, $\eta>1$. The tangential magnetic field direction does not change across such a wave, therefore $\mathbf{b}_2=\mathbf{b}_1$.

Evaluating (9a) and (9b) also from the other side of the reconnecting surface shown in Figure 1 (tilded quantities), the results need to be matched at the contact surface C in the center, i.e.,

$$\eta B_0 = \tilde{\eta}\tilde{B}_0, \tag{10}$$

$$\mathbf{v}_0 - \operatorname{sgn}(mB_n)(\mathbf{v}_{A0}-\mathbf{b}_1 v_{A0} G(\eta)) = \tilde{\mathbf{v}}_0 + \operatorname{sgn}(mB_n) \times (\tilde{\mathbf{v}}_{A0}-\mathbf{b}_1\tilde{v}_{A0}G(\tilde{\eta})), \tag{11}$$

where the fact, $\operatorname{sgn}(\tilde{m}\tilde{B}_n) = -\operatorname{sgn}(mB_n)$, has been used. Defining the vector

$$\mathbf{h} \equiv \operatorname{sgn}(mB_n)(\tilde{\mathbf{v}}_0-\mathbf{v}_0)+\tilde{\mathbf{v}}_{A0}+\mathbf{v}_{A0},$$

solely in terms of the external values of fluid and Alfvén velocities, the solution for $\mathbf{b}_1$ and η (or $\tilde{\eta}$) is

$$\mathbf{b}_1 = \frac{\mathbf{h}}{|\mathbf{h}|}, \tag{12}$$

$$|\mathbf{h}| = v_{A0}G(\eta)+\tilde{v}_{A0}G(\tilde{\eta}). \tag{13}$$

From (10) and (13) η and $\tilde{\eta}$ are obtained and such the solution of the 'low normal flow pressure' Riemannian problem. If there is a zeroth order shear in velocity $\tilde{\mathbf{v}}_0-\mathbf{v}_0 \neq 0$ across T, length and direction of $\mathbf{h}$ will depend on $\operatorname{sgn}(mB_n)$. In this case, the solutions will be different left and right from the reconnection line.

Assuming $B_0<\tilde{B}_0$, the sequence of (shock or self-similar) waves can then be classified as follows:[13]

(i) $|\mathbf{h}|=0$: $T\rightarrow SC\tilde{S}$;

(ii) $0<|\mathbf{h}|<v_{A0}+\tilde{v}_{A0}G(B_0/\tilde{B}_0)$: $T\rightarrow ASC\tilde{S}\tilde{A}$;

(iii) $v_{A0}+\tilde{v}_{A0}G(B_0/\tilde{B}_0)<|\mathbf{h}|<v_{A0}G(\tilde{B}_0/B_0)+\tilde{v}_{A0}$: $T\rightarrow ARC\tilde{S}\tilde{A}$;

(iv) $v_{A0}G(\tilde{B}_0/B_0)+\tilde{v}_{A0}<|\mathbf{h}|<v_{A0}G(\sqrt{2\beta/\gamma+1}) + \tilde{v}_{A0}G(\sqrt{2\tilde{\beta}/\gamma+1})$: $T\rightarrow ARC\tilde{R}\tilde{A}$.

(v) For $|\mathbf{h}|$ approaching the upper limit, cavitation (zero pressure) is reached inside the region between the slow rarefaction waves.

IV. LINEAR ANALYSIS

The non-linear decay of the tangential discontinuity T will cause localized perturbations along the surface defined by T (in the present investigation the xy-plane). These perturbations will excite other MHD waves, in particular fast waves which can propagate transverse to the magnetic field. These waves will modify the surroundings (inflow regions) and induce plasma flows, magnetic field perturbations and a change in plasma pressure.

A. Inflow regions

The small-amplitude perturbations in these regions are obtained from the MHD equations linearized with respect to a constant background. Introducing the displacement vector $\boldsymbol{\xi}(t,\mathbf{x})$, so that first order velocity and magnetic field are given by

$$\mathbf{v}^{(1)}(t,\mathbf{x}) = \left(\frac{\partial}{\partial t}+\mathbf{v}^{(0)}\cdot\nabla\right)\boldsymbol{\xi}(t,\mathbf{x}), \tag{14a}$$

$$\mathbf{B}^{(1)}(t,\mathbf{x}) = \mathbf{B}^{(0)}\cdot\nabla\boldsymbol{\xi}(t,\mathbf{x}) - \mathbf{B}^{(0)}\nabla\cdot\boldsymbol{\xi}(t,\mathbf{x}), \tag{14b}$$

the momentum equation in terms of the displacement vector is

$$\left[\left(\frac{\partial}{\partial t}+\mathbf{v}^{(0)}\cdot\nabla\right)^2-(\mathbf{v}_A^{(0)}\cdot\nabla)^2\right]\boldsymbol{\xi} = -\frac{1}{\rho^{(0)}}\nabla P^{(1)} - \mathbf{v}_A^{(0)} \times (\mathbf{v}_A^{(0)}\cdot\nabla)\nabla\cdot\boldsymbol{\xi}. \tag{15}$$

The first order values for density, $\rho^{(1)}$, pressure, $p^{(1)}$, and total pressure, $P^{(1)}=p^{(1)}+\mathbf{B}^{(0)}\cdot\mathbf{B}^{(1)}/(4\pi)$, may be expressed as functions of the displacement vector $\boldsymbol{\xi}^{(1)}$,

$$\rho^{(1)} = -\rho^{(0)}\nabla\cdot\boldsymbol{\xi},$$

$$p^{(1)} = c_s^2\rho^{(1)},$$

$$\frac{1}{\rho^{(0)}}P^{(1)} = -(v_A^2+c_s^2)\nabla\cdot\boldsymbol{\xi}+(\mathbf{v}_A\cdot\nabla)\mathbf{v}_A\cdot\boldsymbol{\xi}.$$

In order to keep the notation transparent, superscripts for zeroth order values of Alfvén and sound speed will be omitted for the rest of this section.

A Fourier transformation with respect to time t and space components xy is accomplished by the substitution

$$\frac{\partial}{\partial t}+\mathbf{v}^{(0)}\cdot\nabla \rightarrow -i(\omega-\mathbf{v}^{(0)}\cdot\mathbf{k}), \tag{16}$$

$$\nabla \rightarrow (i\mathbf{k}, \mathrm{d}/\mathrm{d}z), \tag{17}$$

where $\mathbf{k}=(k_x,k_y)$. In the following, simply ω is used also for convective time derivatives, but it is to be understood as the Doppler shifted frequency as in (16) when necessary.

After the first order quantities have been substituted into the momentum equation (15), the xy-components $\hat{\boldsymbol{\xi}}(\omega,\mathbf{k},z)$ of the displacement vector can be expressed through the z-component $\zeta(\omega,\mathbf{k},z)$ of the displacement vector, i.e., $\boldsymbol{\xi}=(\hat{\boldsymbol{\xi}},\zeta)$, as

$$\hat{\boldsymbol{\xi}} = -\frac{i}{\Delta}\{\omega^2[(v_A^2+c_s^2)\mathbf{k}-(\mathbf{k}\cdot\mathbf{v}_A)\mathbf{v}_A]-(\mathbf{k}\cdot\mathbf{v}_A)^2c_s^2\mathbf{k}\}\frac{\mathrm{d}\zeta}{\mathrm{d}z}. \tag{18}$$

Here, Δ is the coefficient determinant of the two-dimensional MHD system,

$$\Delta = \omega^4-(v_A^2+c_s^2)k^2\omega^2+(\mathbf{k}\cdot\mathbf{v}_A)^2c_s^2k^2. \tag{19}$$

Introducing useful quantities often used in the Kelvin–Helmholtz analysis of MHD waves,

$$\epsilon = \rho^{(0)}[\omega^2-(\mathbf{k}\cdot\mathbf{v}_A)^2], \tag{20a}$$

Downloaded¬09¬Apr¬2003¬to¬193.170.90.47.¬Redistribution¬subject¬to¬AIP¬license¬or¬copyright,¬see¬http://ojps.aip.org/pop/popcr.jsp

$$q^2=-\frac{\Delta}{\omega^2(v_A^2+c_s^2)-c_s^2(\mathbf{k}\cdot\mathbf{v}_A)^2}, \tag{20b}$$

the total pressure can be expressed in terms of $\zeta(\omega,\mathbf{k},z)$ as

$$P^{(1)}=\frac{\epsilon}{q^2}\frac{\mathrm{d}\zeta}{\mathrm{d}z}. \tag{21}$$

On substituting (18) and (21) into the Fourier transformed z-component of the momentum equation (15), an ordinary differential equation for ζ as a function of z follows,

$$\frac{\mathrm{d}^2\zeta}{\mathrm{d}z^2}-q^2\zeta=0. \tag{22}$$

The present analysis is aimed to study spontaneous reconnection, i.e., there is no inflow of plasma from large distances. The appropriate solutions for each half space and vanishing at infinity are,

$$\zeta(\omega,\mathbf{k},z)=\zeta_0(\omega,\mathbf{k})\mathrm{e}^{-qz},\quad z>0, \tag{23a}$$

$$\tilde{\zeta}(\omega,\mathbf{k},z)=\tilde{\zeta}_0(\omega,\mathbf{k})\mathrm{e}^{\tilde{q}z},\quad z<0. \tag{23b}$$

In the Kelvin–Helmholtz wave analysis, zero mass flux through the boundary requires $\zeta_0=\tilde{\zeta}_0$. In the present study, reconnection gives the boundary an internal structure, i.e., a boundary layer with non-zero mass flux (sink) is formed, and therefore the values for ζ_0 and $\tilde{\zeta}_0$ will be different.

The total pressure perturbations in the upper and the lower half spaces are

$$P^{(1)}=-\frac{\epsilon}{q}\zeta,\quad \tilde{P}^{(1)}=\frac{\tilde{\epsilon}}{\tilde{q}}\tilde{\zeta}, \tag{24}$$

so that first order total pressure balance across the boundary layer at $z=0$ connects the solutions by the condition

$$\frac{\epsilon}{q}\zeta_0+\frac{\tilde{\epsilon}}{\tilde{q}}\tilde{\zeta}_0=0. \tag{25}$$

Defining the quantities,

$$L\equiv\frac{\epsilon}{q},\quad \tilde{L}\equiv\frac{\tilde{\epsilon}}{\tilde{q}},\quad Q\equiv\zeta_0-\tilde{\zeta}_0,$$

the solutions for the z-displacement in the upper and lower half space are,

$$\zeta(\omega,\mathbf{k},z)=\frac{\tilde{L}\mathrm{e}^{-qz}}{L+\tilde{L}}Q(\omega,\mathbf{k}), \tag{26a}$$

$$\tilde{\zeta}(\omega,\mathbf{k},z)=-\frac{L\mathrm{e}^{\tilde{q}z}}{L+\tilde{L}}Q(\omega,\mathbf{k}). \tag{26b}$$

The source function $Q\equiv\zeta_0-\tilde{\zeta}_0$ will be obtained in the next section by solving the initial value problem for the linear wave propagation inside the boundary layer (normal component analysis).

It may be observed that $L+\tilde{L}=0$ is the dispersion relation studied in the analysis of hydromagnetic surface waves[35] and Kelvin–Helmholtz instability of surface perturbations.[36] The driving source of this instability is the velocity shear contained in the Doppler shifted frequency. Any additional magnetic tension, in general, counteracts this instability and has a stabilizing effect. In the present context, stability with respect to Kelvin–Helmholtz waves (ideal instability) is assumed. Instead, the appearance of magnetic reconnection (resistive instability) is investigated.

B. Boundary layer

From (2b) and (2d), respectively, from (6b) and (6d) it follows that the ratio of mass flux and normal magnetic field is already determined by the change of density and tangential magnetic field $\mathbf{B}_t$ across any discontinuities with $B_n\neq 0$ as[13]

$$\frac{m}{B_n}=\begin{cases}\pm\sqrt{\dfrac{\rho}{4\pi}} & (A),\\ \pm\dfrac{1}{\sqrt{4\pi}}\sqrt{\dfrac{[\![\mathbf{B}_t]\!]}{[\![\mathbf{B}_t/\rho]\!]}} & (S),\\ \pm\sqrt{\dfrac{\rho}{4\pi}}\dfrac{1}{\sqrt{1+v_A^2/c_s^2}} & (R),\end{cases} \tag{27}$$

where the sign has to be chosen according to the relative orientation of mass flux and magnetic field through the discontinuity.

Evidently, a second relation between the mass flux m and the normal magnetic field B_n at every point along the boundary is needed. Again, let a moving surface with unit normal $\mathbf{n}$ and speed u be defined by $\varphi(t,\mathbf{x})=0$ as in (5) so that

$$m=\frac{\rho}{|\nabla\varphi|}\left(\frac{\partial}{\partial t}+\mathbf{v}\cdot\nabla\right)\varphi, \tag{28a}$$

$$B_n=\frac{1}{|\nabla\varphi|}\mathbf{B}\cdot\nabla\varphi. \tag{28b}$$

The electric field tangential to the surface in the rest frame of the surface is given by

$$\mathbf{E}_t^*=-\frac{1}{c}\mathbf{n}\times[(\mathbf{v}-u\mathbf{n})\times\mathbf{B}]=-\frac{B_n}{c}(\mathbf{w}-u\mathbf{n})=-\frac{B_n}{c}\mathbf{w}_t, \tag{29}$$

where the velocity

$$\mathbf{w}\equiv\mathbf{v}-\frac{m}{\rho B_n}\mathbf{B}, \tag{30}$$

has been defined. Clearly, $\mathbf{w}_t$ is an invariant across any surface with $B_n\neq 0$, including rotational discontinuities and shock waves. It also follows that $\mathbf{w}\cdot\mathbf{n}=u$, and therefore the location of the surface satisfies the equation

$$\left(\frac{\partial}{\partial t}+\mathbf{w}\cdot\nabla\right)\varphi=0. \tag{31}$$

The electric field $E^*(t,y)$ along the line which is formed by the cross section of the surface $\varphi(t,\mathbf{x})=0$ with the plane $x=0$ is

$$E^*(t,y)=(\mathbf{n}\times\mathbf{e}_x)\cdot\mathbf{E}^*=-\mathbf{E}_t^*\cdot\mathbf{e}_x=\frac{B_n}{c}(w_x-un_x). \tag{32}$$

Downloaded¬09¬Apr¬2003¬to¬193.170.90.47.¬Redistribution¬subject¬to¬AIP¬license¬or¬copyright,¬see¬http://ojps.aip.org/pop/popcr.jsp

For a thin boundary layer at $z=0$, it is advantageous to separate the z-dependence of $\varphi(t,\mathbf{x})$ explicitly,

$$\varphi(t,x,y,z)=z-f(t,x,y), \tag{33}$$

where $f(t,x,y)$ is a first order quantity and $|\nabla\varphi|=1+\mathcal{O}(\varepsilon)$.

In terms of the z-component of the displacement vector $\zeta(t,\mathbf{x})$, the first order z-components of velocity and magnetic field are

$$v_z^{(1)}(t,\mathbf{x})=\left(\frac{\partial}{\partial t}+\mathbf{v}^{(0)}\cdot\nabla\right)\zeta(t,\mathbf{x}), \tag{34a}$$

$$B_z^{(1)}(t,\mathbf{x})=\mathbf{B}^{(0)}\cdot\nabla\zeta(t,\mathbf{x}). \tag{34b}$$

It then follows from (31) and (33) in first order,

$$w_z^{(1)}-\left(\frac{\partial}{\partial t}+\mathbf{w}^{(0)}\cdot\nabla\right)f=0. \tag{35}$$

Using (30) and (34b), $w_z^{(1)}$ can also be expressed solely in terms of the z displacement,

$$w_z^{(1)}=\left(\frac{\partial}{\partial t}+\mathbf{w}^{(0)}\cdot\nabla\right)\zeta, \tag{36}$$

and the first order partial differential equation

$$\left(\frac{\partial}{\partial t}+\mathbf{w}^{(0)}\cdot\nabla\right)(f-\zeta)=0, \tag{37}$$

for $f-\zeta$ is obtained. The solution is conveniently expressed through an arbitrary function Φ whose arguments are constants of motion,

$$f(t,x,y)=\zeta(t,x,y)+\Phi\left(t-\frac{x}{w_x^{(0)}},y-\frac{w_y^{(0)}}{w_x^{(0)}}x\right). \tag{38}$$

The normal magnetic field can now be expressed in terms of this function Φ,

$$\begin{aligned}B_n&=B_z^{(1)}-\mathbf{B}^{(0)}\cdot\nabla f\\&=-\mathbf{B}^{(0)}\cdot\nabla\Phi\\&=\frac{c}{w_x^{(0)}}\left(\frac{B_x^{(0)}}{c}\frac{\partial\Phi}{\partial t}+E_z^{(0)}\frac{\partial\Phi}{\partial y}\right),\end{aligned} \tag{39}$$

where

$$E_z^{(0)}=\frac{1}{c}(w_y^{(0)}B_x^{(0)}-w_x^{(0)}B_y^{(0)})\equiv\frac{1}{c}(v_y^{(0)}B_x^{(0)}-v_x^{(0)}B_y^{(0)}). \tag{40}$$

In (39), $\partial\Phi/\partial t$ and $\partial\Phi/\partial y$ indicate derivatives of function Φ with respect to the first and second argument respectively. If this result for B_n is evaluated at $x=0$ and used in (32), the following equation for Φ is obtained:

$$\frac{B_x^{(0)}}{c}\frac{\partial\Phi}{\partial t}+E_z^{(0)}\frac{\partial\Phi}{\partial y}=E^*(t,y). \tag{41}$$

In the present study, the reconnection line is assumed to be located in the plane $x=0$. Also, the electric field $E^*(t,y)$ tangential to the reconnection line is assumed to be known. It is important to note that the reconnection line must be allowed to move in the plane $x=0$. This movement is not a free parameter, rather it will be obtained self-consistently as a part of the complete solution. The solution of (41) is,

$$\Phi(t,y)=\frac{c}{B_x^{(0)}}\int_0^t \mathrm{d}\tau E^*\left[\tau,y-\frac{cE_z^{(0)}}{B_x^{(0)}}(t-\tau)\right]. \tag{42}$$

This, together with (38), is a central result for the present reconnection problem. It allows us to determine the B_n distribution over any specified surface along the boundary for all times in terms of the reconnection electric field $E^*(t,y)$.

The function $f(t,x,y)$ identifies the location of the discontinuities and therefore it must be unique if (38) is evaluated at the different sides of the discontinuities. These conditions give the connections between the z-components of the displacement vector in the different regions

$$\begin{aligned}&\zeta_0+\Phi_0(\mathbf{w}_A^{(0)})=\zeta_1+\Phi_1(\mathbf{w}_A^{(0)}) \quad (A),\\&\zeta_1+\Phi_1(\mathbf{w}_S^{(0)})=\zeta_2+\Phi_2(\mathbf{w}_S^{(0)}) \quad (S),\\&\zeta_2+\Phi_2(\mathbf{v}_2^{(0)})=\tilde{\zeta}_2+\tilde{\Phi}_2(\tilde{\mathbf{v}}_2^{(0)}) \quad (C),\\&\tilde{\zeta}_1+\tilde{\Phi}_1(\tilde{\mathbf{w}}_S^{(0)})=\tilde{\zeta}_2+\tilde{\Phi}_2(\tilde{\mathbf{w}}_S^{(0)}) \quad (\tilde{S}),\\&\tilde{\zeta}_0+\tilde{\Phi}_0(\tilde{\mathbf{w}}_A^{(0)})=\tilde{\zeta}_1+\tilde{\Phi}_1(\tilde{\mathbf{w}}_A^{(0)}) \quad (\tilde{A}),\end{aligned} \tag{43}$$

where the short hand notation,

$$\Phi_i(\mathbf{w}^{(0)})\equiv\Phi_i\left(t-\frac{x}{w_x^{(0)}},y-\frac{w_y^{(0)}}{w_x^{(0)}}x\right), \tag{44}$$

evaluated with (42) in region i (see Figure 1), has been used. Notice, that velocity $\mathbf{v}_2$, magnetic field $\mathbf{B}_2$, as well as the pressure p_2 are continuous across the contact surface C separating regions 2 and $\tilde{2}$. Therefore, ζ and Φ are continuous as well.

In order to obtain such a connection through a rarefaction wave, consider the tangent planes through points in two neighboring wave surfaces. If the magnetic field is continuous, magnetic flux conservation through the surface of an infinitesimal wedge shaped volume defined by the planes and their intersection line, gives a local relation between changes in normal vector and normal magnetic field,

$$\mathrm{d}B_n=\mathbf{B}\cdot\mathrm{d}\mathbf{n}. \tag{45}$$

If these changes are expressed in terms of f, ζ and Φ,

$$\begin{aligned}&\mathrm{d}\mathbf{n}=-\nabla\mathrm{d}f,\\&\mathrm{d}B_n=-\mathrm{d}(\mathbf{B}^{(0)}\cdot\nabla(f-\zeta))\\&\qquad=-\mathrm{d}\mathbf{B}^{(0)}\cdot\nabla\Phi-\mathbf{B}^{(0)}\cdot\nabla(\mathrm{d}f-\mathrm{d}\zeta),\end{aligned}$$

and together with (9a) are substituted into (45) it follows,

$$\mathbf{B}^{(0)}\cdot\nabla[\eta\mathrm{d}\zeta-\Phi_\eta(\mathbf{w}_R^{(0)}(\eta))\mathrm{d}\eta]=0, \tag{46a}$$

or equivalently,

$$\mathrm{d}\zeta=\frac{1}{\eta}\Phi_\eta(\mathbf{w}_R^{(0)}(\eta))\mathrm{d}\eta. \tag{46b}$$

The solution is the desired connection between ζ_1 and ζ_2,

$$\zeta_2=\zeta_1+\int_1^\eta\frac{\mathrm{d}\eta'}{\eta'}\Phi_{\eta'}(\mathbf{w}_R^{(0)}(\eta')) \quad (R). \tag{47}$$

Downloaded¬09¬Apr¬2003¬to¬193.170.90.47.¬Redistribution¬subject¬to¬AIP¬license¬or¬copyright,¬see¬http://ojps.aip.org/pop/popcr.jsp

The function Φ in this expression has to be evaluated in the form of (44) together with the η-dependent zeroth order values within the rarefaction wave in (42), namely,

$$\Phi_\eta(t,y)=\frac{c}{B_x^{(0)}(\eta)}\int_0^t \mathrm{d}\tau E^*\left[\tau, y-\frac{cE_z^{(0)}(\eta)}{B_x^{(0)}(\eta)}(t-\tau)\right]. \tag{48}$$

C. Matching solutions

From the results of the last section it is possible to express the source term $Q(t,x,y)=\zeta_0(t,x,y)-\tilde{\zeta}_0(t,x,y)$ in (26b) as a functional of the electric field along the reconnection line in its rest frame located in the plane $x=0$. This electric field is likely to be determined from non-ideal processes leading to some effective finite conductivity. In the present ideal MHD analysis, the reconnection electric field is assumed to be a known function.

From (43) and (47) the source term is obtained as

$$Q=\Delta_A+\Delta_{S(R)}-(\tilde{\Delta}_A+\tilde{\Delta}_{S(R)}), \tag{49a}$$

$$\Delta_A\equiv\Phi_1(\mathbf{w}_A^{(0)})-\Phi_0(\mathbf{w}_A^{(0)}), \tag{49b}$$

$$\Delta_S\equiv\Phi_2(\mathbf{w}_S^{(0)})-\Phi_1(\mathbf{w}_S^{(0)}), \tag{49c}$$

$$\Delta_R\equiv-\int_1^\eta\frac{\mathrm{d}\eta'}{\eta'}\Phi_{\eta'}(\mathbf{w}_R^{(0)}(\eta')). \tag{49d}$$

Similar expressions hold for $\tilde{\Delta}_A$ and $\tilde{\Delta}_{S(R)}$.

The contribution of each term has the same character in form of a time and space shifted function

$$\Phi\left(t-\frac{x}{w_x},y-\frac{w_y}{w_x}x\right). \tag{50}$$

In (26b) the Fourier transformed source term is needed. In view of handling correctly the initial value problem, at this point it is more convenient to use Laplace instead of Fourier transform with respect to time. The Laplace Fourier transform of a time and space shifted causal function, $\Phi(t,y)\equiv 0$ for $t<0$, is

$$\begin{aligned}\mathscr{L}_t\mathscr{F}_{xy}&\left\{\Phi^\pm\left(t-\frac{x}{w_x^\pm},y-\frac{w_y^\pm}{w_x^\pm}x\right)\right\}\\&=\int_0^\infty \mathrm{d}t\mathrm{e}^{-pt}\int_{R^2}\mathrm{d}x\mathrm{e}^{-i\mathbf{k}\cdot\mathbf{x}}\Phi^\pm\left(t-\frac{x}{w_x^\pm},y-\frac{w_y^\pm}{w_x^\pm}x\right)\\&\quad\times\Theta\left(t-\frac{x}{w_x^\pm}\right)\Theta(\pm x)\\&=\pm\frac{w_x^\pm}{p+i\mathbf{w}^\pm\cdot\mathbf{k}}\Phi^\pm(p,k_y).\end{aligned} \tag{51}$$

Here, the possibly discontinuous behavior of Φ at $x=0$ [see (42)], has been accounted for by an additional Heaviside step function $\Theta(\pm x)$, as well as the different values of $\mathbf{w}^\pm$ for $x>0$ and $x<0$.

Let Green's functions be defined for the contributions to the source term Q of each single wave, e.g., the upper Alfvén wave A, like

$$G_A^+(p,\mathbf{k},z)=\frac{\tilde{L}\mathrm{e}^{-qz}}{L+\tilde{L}}\frac{w_{Ax}^+}{p+i\mathbf{w}_A^+\cdot\mathbf{k}},\quad x>0, \tag{52a}$$

$$G_A^-(p,\mathbf{k},z)=-\frac{\tilde{L}\mathrm{e}^{-qz}}{L+\tilde{L}}\frac{w_{Ax}^-}{p+i\mathbf{w}_A^-\cdot\mathbf{k}},\quad x<0. \tag{52b}$$

Here, $\mathbf{w}_A^+$ and $\mathbf{w}_A^-$ have to be evaluated from the zeroth order components at the upper Alfvén wave for $x>0$ and $x<0$ respectively.

In terms of these Green's functions the contribution of source A to the complete solution can be expressed as the double folding integral

$$\begin{aligned}\zeta_A(t,\boldsymbol{x})=\int_0^t\mathrm{d}\tau\int_{-\infty}^\infty\mathrm{d}\eta[&G_A^+(t-\tau,x,y\\&-\eta,z)\Phi_A^+(\tau,\eta)\Theta(x)\\&+G_A^-(t-\tau,x,y-\eta,z)\Phi_A^-(\tau,\eta)\Theta(-x)],\end{aligned} \tag{53}$$

where $\Phi_A^\pm(t,y)\equiv\Phi_1^\pm(t,y)-\Phi_0^\pm(t,y)$ and the space-time Green's function is obtained from the inverse Laplace Fourier transform,

$$\begin{aligned}G_A^\pm(t,x,y,z)=\int_{-i\infty+\sigma}^{i\infty+\sigma}\frac{\mathrm{d}p}{2\pi}\mathrm{e}^{\,pt}\int_{R^2}\frac{\mathrm{d}k}{(2\pi)^2}\mathrm{e}^{\,i\mathbf{k}\cdot\mathbf{x}}\\\times G_A^\pm(p,k_x,k_y,z),\quad\sigma>0.\end{aligned} \tag{54}$$

Thus, the complete solution for the upper half space $z>0$ is the sum,

$$\zeta=\sum_{i=A,S(R),\tilde{S}(\tilde{R}),\tilde{A}}\zeta_i. \tag{55}$$

In case of a rarefaction wave, an additional integration over η is needed,

$$\zeta_R^\pm(p,\mathbf{k},z)=\pm\frac{\tilde{L}\mathrm{e}^{-qz}}{L+\tilde{L}}\int_1^\eta\mathrm{d}\eta'\frac{w_{Rx}^\pm(\eta')}{p+i\mathbf{w}_R^\pm(\eta')\cdot\mathbf{k}}\Phi_{\eta'}(p,k_y).$$

V. COMPRESSIBLE RECONNECTION IN PLANE GEOMETRY

In plane geometry, the general formalism of the last section can be worked out further. In particular, it is possible to do the inversion of the Laplace Fourier transform in closed form by rearranging the contour in the complex plane $s=kv_A/p$, i.e., the inverse normalized phase velocity. In this way, the Green's function of the system is obtained. It describes the exact linear compressible wave motions in the plane $y=0$ driven by sources moving along the x axis.

The sources are created by magnetic reconnection locally, i.e., along the reconnection line in the plane $x=0$. Magnetic shear energy is released and MHD waves are launched and propagate along the current sheet. These waves induce the decay of the tangential discontinuity into shock waves also away from the reconnection site. The clue of the rapid reconnection model is that the amount of dissipation within the shock waves is independent of the dissipation mechanism. Rather it is determined by the upstream and downstream boundary conditions. Only for the width of the

Downloaded¬09¬Apr¬2003¬to¬193.170.90.47.¬Redistribution¬subject¬to¬AIP¬license¬or¬copyright,¬see¬http://ojps.aip.org/pop/popcr.jsp

shocks is knowledge about the actual dissipation mechanism required. On the other hand, the tangential electric field generated along the reconnection line by finite conductivity is carried by shear waves along the current sheet. In the absence of an externally driven inflow, the boundary conditions of 'spontaneous reconnection' are essentially given by this electric field. It determines the magnetic flux being reconnected at the reconnection line as well as the stand off distance between the shock waves and thus the plasma volume being processed (accelerated and heated) through the shocks.

A. Basic parameters

In order to keep the numerics of the non-linear part simple, let us be given the following ratios of magnetic fields:

$$\mu \equiv \frac{B_0}{\tilde{B}_0} = \sqrt{\frac{2\tilde{\beta}/\gamma+1}{2\beta/\gamma+1}}, \quad \tilde{\eta} \equiv \frac{\tilde{B}_2}{\tilde{B}_0} \equiv \frac{B_2}{\tilde{B}_0},$$

where $2\beta/\gamma \equiv 8\pi p_0/B_0^2$ and the adiabatic number is assumed to be $\gamma = 5/3$. The external conditions are assumed to be such that no rarefaction waves are needed and that the Alfvén speed in the upper half plane, $z>0$, is less than the Alfvén speed in the lower half plane, $z<0$. In plane geometry, only one Alfvén discontinuity is needed which rotates the magnetic field through 180°. This always happens at the side with the lower Alfvén speed. In the present investigation, this side is assumed to be the upper half plane (see top panel of Figure 4). From these numbers all other values follow,

$$\eta \equiv \frac{B_2}{B_0} = \frac{\tilde{\eta}}{\mu}, \tag{56a}$$

$$\nu \equiv \frac{\rho_2}{\rho_0} = 1 + \frac{1-\eta^2}{2\beta+(\gamma-1)(1-\eta)}, \tag{56b}$$

$$\tilde{\nu} \equiv \frac{\tilde{\rho}_2}{\tilde{\rho}_0} = 1 + \frac{1-\tilde{\eta}^2}{2\tilde{\beta}+(\gamma-1)(1-\tilde{\eta})}, \tag{56c}$$

$$\mathbf{w}_A^{\pm} = \pm \mathbf{v}_{A0}, \tag{56d}$$

$$\mathbf{w}_S^{\pm} = \pm \left(2 - \sqrt{\frac{1-\eta/\nu}{1-\eta}}\right) \mathbf{v}_{A0}, \tag{56e}$$

$$\tilde{\mathbf{v}}_2^{\pm} = \pm (2 - \sqrt{(1-\eta)(1-\eta/\nu)}) \mathbf{v}_{A0}, \tag{56f}$$

$$\tilde{\mathbf{w}}_S^{\pm} = \mp \sqrt{\frac{1-\tilde{\eta}/\tilde{\nu}}{1-\tilde{\eta}}} \tilde{\mathbf{v}}_{A0}. \tag{56g}$$

Notice that the velocities $\mathbf{w}$ are different for $x>0$ and $x<0$, i.e., right and left of the reconnection line, because $\mathrm{sgn}(mB_n)$ changes sign. In the present example without zeroth order shear motion this is just effected by a change in sign.

In plane geometry with anti-directional fields and no shear in velocity, (42) reduces to

$$\Phi(t) = \frac{c}{B_x^{(0)}} \int_0^t \mathrm{d}\tau E^*(\tau), \tag{57}$$

so that all Φ functions can conveniently be expressed in terms of Φ_0 as

$$\Phi_0(t) = \frac{c}{B_0} \int_0^t \mathrm{d}\tau E^*(\tau), \tag{58a}$$

$$\Phi_1(t) = -\Phi_0(t), \tag{58b}$$

$$\Phi_2(t) = \tilde{\Phi}_2(t) = -\frac{1}{\eta}\Phi_0(t), \tag{58c}$$

$$\tilde{\Phi}_0(t) = -\mu\Phi_0(t), \tag{58d}$$

valid for $x>0$ as well as for $x<0$. Therefore, it follows from (49a) for the source function,

$$Q(t,x) = -2\Phi_0\left(t - \frac{|x|}{w_A}\right) + \left(1 - \frac{1}{\eta}\right)\Phi_0\left(t - \frac{|x|}{w_S}\right) - \left(\mu - \frac{1}{\eta}\right)\Phi_0\left(t - \frac{|x|}{\tilde{w}_S}\right), \tag{59a}$$

valid along the whole x axis. From (51), adding the contributions for $x<0$ and $x>0$, the Laplace Fourier transform is,

$$Q(p,k) = \left[-2\frac{2pw_A}{p^2+w_A^2k^2} + \left(1 - \frac{1}{\eta}\right)\frac{2pw_S}{p^2+w_S^2k^2} - \left(\mu - \frac{1}{\eta}\right)\frac{2p\tilde{w}_S}{p^2+\tilde{w}_S^2k^2}\right]\Phi_0(p). \tag{59b}$$

B. Solution in Laplace Fourier space

From (43), the z displacements in the different regions of the boundary layer $z=0$ are connected as

$$\zeta_1(t,x) = \zeta_0(t,x) + 2\Phi_0\left(t - \frac{|x|}{v_{A0}}\right), \tag{60a}$$

$$\zeta_2(t,x) = \zeta_1(t,x) - \left(1 - \frac{1}{\eta}\right)\Phi_0\left(t - \frac{|x|}{w_S}\right), \tag{60b}$$

$$\tilde{\zeta}_0(t,x) = \zeta_0(t,x) - Q(t,x). \tag{60c}$$

The shock waves are located at

$$f_A(t,x) = \zeta_0(t,x) + \Phi_0\left(t - \frac{|x|}{v_{A0}}\right), \tag{61a}$$

$$f_S(t,x) = \zeta_1(t,x) - \Phi_0\left(t - \frac{|x|}{w_S}\right), \tag{61b}$$

$$f_C(t,x) = \zeta_2(t,x) - \frac{1}{\eta}\Phi_0\left(t - \frac{|x|}{v_2}\right), \tag{61c}$$

$$\tilde{f}_S(t,x) = \tilde{\zeta}_0(t,x) - \mu\Phi_0\left(t - \frac{|x|}{\tilde{w}_S}\right). \tag{61d}$$

The separatrices are found by considering the amount of reconnected flux, i.e.,

$$f_{sep}(t,x) = \zeta_0(t,x) + \Phi_0(t), \tag{62a}$$

$$\tilde{f}_{sep}(t,x) = \tilde{\zeta}_0(t,x) - \mu\Phi_0(t). \tag{62b}$$

Downloaded¬09¬Apr¬2003¬to¬193.170.90.47.¬Redistribution¬subject¬to¬AIP¬license¬or¬copyright,¬see¬http://ojps.aip.org/pop/popcr.jsp

It is easily checked that in the plane $x=0$ all discontinuities and separatrices intersect in a unique (reconnection) line,

$$f_A(t,0)=f_S(t,0)=f_C(t,0)=\tilde{f}_S(t,0)=f_{sep}(t,0)$$
$$=\tilde{f}_{sep}(t,0)=\zeta_0(t,0)+\Phi_0(t).$$

In plane geometry and setting $\omega=ip$, (20a) and (20b) reduce to

$$\epsilon=-\rho_0 p^2(1+k^2 v_{A0}^2/p^2), \tag{63a}$$

$$q=\frac{p}{v_{A0}}\sqrt{\frac{(1+k^2v_{A0}^2/p^2)(1+\beta k^2 v_{A0}^2/p^2)}{1+\beta+\beta k^2 v_{A0}^2/p^2}}, \tag{63b}$$

where $\beta\equiv c_{s0}^2/v_{A0}^2$. Similar expressions are valid for tilded quantities.

This completes the solution (26b) for $\zeta(p,k,z)$ and $\tilde{\zeta}(p,k,z)$ in Laplace Fourier space.

C. Green's function

The following method, established in Ref. 31 (see also Refs. 37, 38 and references therein), allows one to obtain the inverse of the system response function in closed form. Here, the method is generalized and put in such a way that it can be used for linear plane wave problems including three (MHD case) or, maybe, even more anisotropic wave modes. In general, all these waves will be coupled either intrinsically, e.g., like the fast and slow MHD wave modes, or by boundary conditions, e.g., pressure balance along the interface of two different media.

In a first step, the inverse Fourier transform with respect to k is rewritten using the symmetry $\zeta(p,k,z)=\zeta(p,-k,z)$ as

$$\zeta(p,x,z)=\int_{-\infty}^{\infty}\frac{dk}{2\pi}e^{ikx}\zeta(p,k,z)$$
$$=\frac{1}{\pi}\Re\int_0^{\infty}dk e^{-ikx}\zeta(p,k,z).$$

Introducing the inverse phase velocity s and polar coordinates as new variables

$$s=\frac{kv_{A0}}{p},\quad x=r\ \sin\ \vartheta,\quad z=r\ \cos\ \vartheta, \tag{64}$$

the integral becomes

$$\zeta(p,x,z)=\Re\frac{1}{\pi}\int_0^{\infty}ds\frac{\tilde{\bar{L}}(s^2)}{\bar{L}(s^2)+\tilde{\bar{L}}(s^2)}\bar{Q}(s^2)\ e^{-p\tau(s)}\Phi_0(p), \tag{65}$$

with

$$\bar{L}(s^2)=-(1+s^2)\sqrt{\frac{1+1/\beta+s^2}{(1+s^2)(1/\beta+s^2)}}, \tag{66a}$$

$$\tilde{\bar{L}}(s^2)=-\frac{1}{\mu^2}(\gamma_A^2+s^2)\sqrt{\frac{\gamma_A^2(1+1/\beta)+s^2}{(\gamma_A^2+s^2)(\gamma_A^2/\beta+s^2)}}, \tag{66b}$$

$$\tau(s)=\frac{r}{v_{A0}}[\bar{q}(s^2)\cos\ \vartheta+is\ \sin\ \vartheta], \tag{66c}$$

$$\bar{q}(s^2)=\sqrt{\frac{(1+s^2)(1/\beta+s^2)}{1+1/\beta+s^2}}, \tag{66d}$$

$$\bar{Q}(s^2)=2\left[-2\frac{1}{s^2+1}+\left(1-\frac{1}{\eta}\right)\frac{\gamma_A/\gamma_S}{s^2+(\gamma_A^2/\gamma_S^2)}\right.$$
$$\left.-\left(\mu-\frac{1}{\eta}\right)\frac{\gamma_A/\tilde{\gamma}_S}{s^2+(\gamma_A^2/\tilde{\gamma}_S^2)}\right], \tag{66e}$$

where the ratios $\gamma_A\equiv v_{A0}/\tilde{v}_{A0}$, $\gamma_S\equiv w_S/\tilde{v}_{A0}$, and $\tilde{\gamma}_S\equiv\tilde{w}_S/\tilde{v}_{A0}$ have been defined.

If it is possible to deform the contour in the complex s plane in such a way that $\tau(s)$ is real along the path of integration, the inverse Laplace transform

$$\mathscr{L}^{-1}\{e^{-p\tau}\Phi(p)\}=\Phi(t-\tau) \tag{67}$$

is well defined for all $\tau(s)$.

The poles of $\bar{Q}(s^2)$ as well as the branch points of $\bar{L}(s^2)$ and $\tilde{\bar{L}}(s^2)$ are located on the imaginary axis of the complex s plane. In addition, the integrand is exponentially bounded for $\Im\{s\}<0$. Therefore, the contour can be deformed from the real axis into the fourth quadrant of the complex s plane if the branch cuts are put left of the imaginary axis.

Setting $\tau=t$, the inversion of (66c), i.e., the solution of

$$s^4+2i\tau_0\ \sin\ \vartheta s^3+\left(1+\frac{1}{\beta}-\tau_0^2\right)s^2+\left(1+\frac{1}{\beta}\right)2i\tau_0\ \sin\ \vartheta s$$
$$+\frac{\cos^2\ \vartheta}{\beta}-\left(1+\frac{1}{\beta}\right)\tau_0^2=0, \tag{68}$$

with $\tau_0\equiv v_{A0}t/r$ defines the end point of integration s_{max} from causality, $\Phi_0(t)\equiv 0$ for $t<0$. The root of the quartic which lies in the fourth quadrant on the contour for real $\tau(s)$ has to be taken.

The displacement in space time is then given by the integral

$$\zeta(t,x,z)=\Re\frac{1}{\pi}\int_{\mathscr{C}}ds\frac{\tilde{\bar{L}}(s^2)}{\bar{L}(s^2)+\tilde{\bar{L}}(s^2)}\bar{Q}(s^2)\Phi_0(t-\tau(s)), \tag{69}$$

where $\mathscr{C}$ is that contour from $s=0$ to $s=s_{max}$ where $\tau(s)$ is real. Contours for different plasma parameters are shown in Figure 2. After a variable transformation from s to τ the solution can finally be written as a convolution with a Green's function as

$$\zeta(t,x,z)=\int_{\tau_{min}}^{t}d\tau G(\tau,x,z)\Phi_0(t-\tau), \tag{70}$$

$$G(\tau,x,z)=\Re\frac{1}{\pi}\frac{ds}{d\tau}\frac{\tilde{\bar{L}}(s^2(\tau))}{\bar{L}(s^2(\tau))+\tilde{\bar{L}}(s^2(\tau))}\bar{Q}(s^2(\tau)), \tag{71}$$

Downloaded¬09¬Apr¬2003¬to¬193.170.90.47.¬Redistribution¬subject¬to¬AIP¬license¬or¬copyright,¬see¬http://ojps.aip.org/pop/popcr.jsp

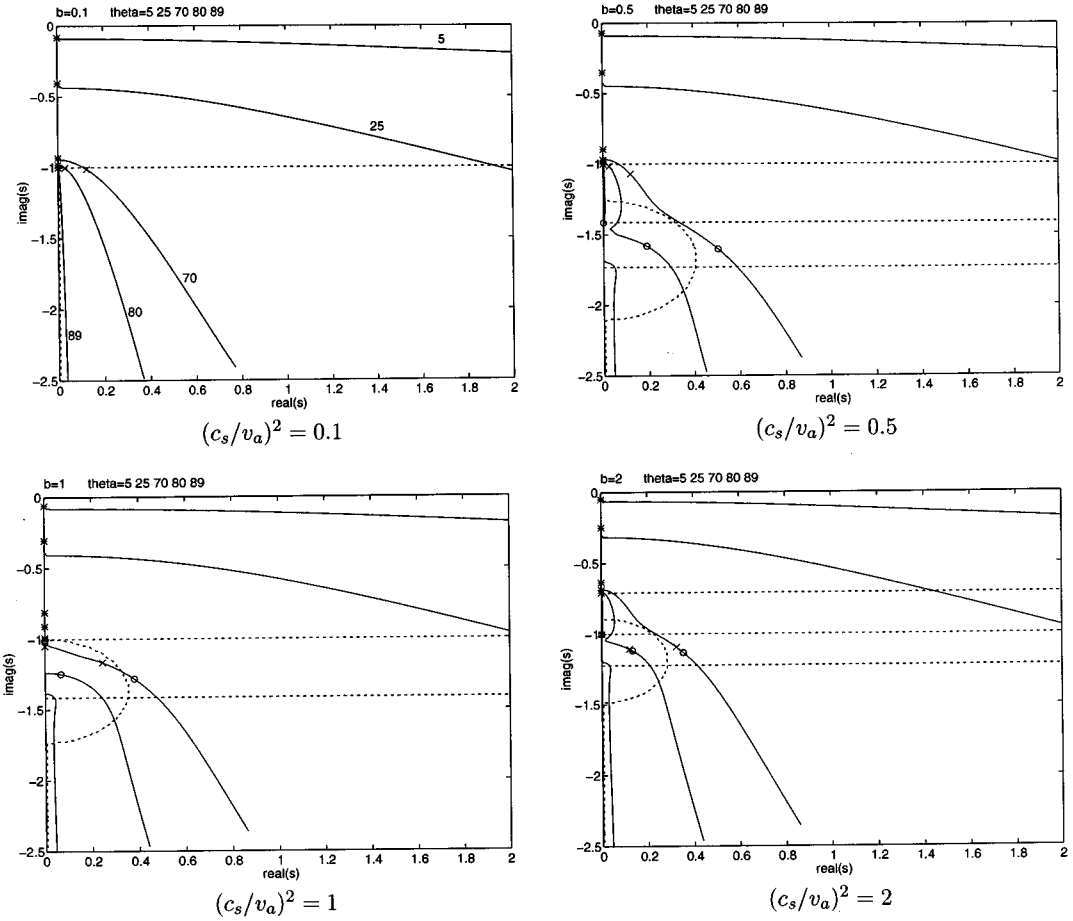

FIG. 2. Contours of real $\tau(s)$ and different ϑ values defined in (64) in the complex s plane. The point $s\to 0$ corresponds to $r\to\infty$ in real space. The end point of integration s_{max} for given t, r, and ϑ is the solution of the quartic (68) in the fourth quadrant. The asterisk, cross, and circle correspond to the location of the fast, Alfvén, and slow wave front on the contour. The intersection points of the dotted straight lines with the imaginary axis are branch points. The dotted circle is the locus where the imaginary part of the argument of the square root of $L(s^2)$ vanishes. Within this circle, i.e., for $\vartheta \geqslant 70°$ (direction parallel to the background magnetic field), the influence of Alfvén and slow wave on the fast wave is most prominent.

$$\tau_{min} = \frac{r}{v_{A0}} \sqrt{\frac{1}{1+\beta}} \cos\ \vartheta. \tag{72}$$

The discussion of the Green's function is simpler if there is only one wave with isotropic properties present. In this case, the contour in the s plane is an exact hyperbola. This is also true for the general case in the limit $\vartheta\to 0$ (direction perpendicular to the background field) as well as in the limit $\beta\to 0$ as can be observed in Figure 2. For a subsonic source, the Green's function is identical to zero from $s=0$ up to the point $s=s_{min}$ which corresponds to points at the wave front $\tau(s_{min})=r/v$. In the isotropic single wave case, the point $s=s_{min}$ coincides with the point where the contour leaves the imaginary axis. In the general case depicted in Figure 2, the fast wave front is indicated by an asterisk. The end point of integration $\tau(s_{max})=t$ is determined by causality and lies somewhere in the fourth quadrant.

For a supersonic source, there exist also perturbations within the Mach cone in front of the wave front. In the complex s plane of Figure 2, this is reflected in non-zero contributions to the integral from the contour along the imaginary axis between $s=0$ and the fast wave front (asterisk). Pressure balance at an interface with higher wave speed in the other half space will always produce a supersonic source. The perturbed region along such an interface with pressure balance is known as side wave.

In the general case, the anisotropic propagation characteristics and the coupling of the waves make the picture much more complex. Perturbations might be super and subsonic with respect to different wave speeds at the same time even in the same half space. The result is a deformation of the contour in the interaction region as can be seen in Figure 2. Because Alfvén and slow waves propagate mainly in the direction of the magnetic field, the effect is most prominent for large ϑ, i.e., near the x axis in real space. In the limit $\beta\to 0$, the lower two branch points go to minus infinity and the isotropic single wave limit is obtained. Below, these effects will be discussed further in connection with specific solutions for magnetic reconnection.

However, instead of performing the integration from $s=0$ to $s=s_{max}$ along the contour where $\tau(s)$ is real, in practice it is more advantageous to deform the contour within the region of analyticity to a curve with simpler parametrization, e.g., an arc connecting the points $s=0$ and $s=s_{max}$. This can always be done as long as the source

Downloaded¬09¬Apr¬2003¬to¬193.170.90.47.¬Redistribution¬subject¬to¬AIP¬license¬or¬copyright,¬see¬http://ojps.aip.org/pop/popcr.jsp

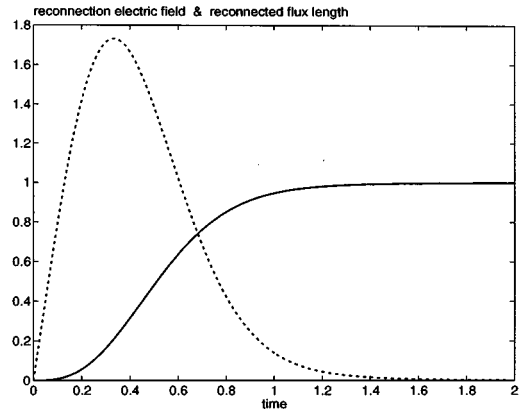

FIG. 3. Assumed time behavior of the reconnection electric field, $E^*(t)$ (dotted) and the reconnected flux length, $\Phi(t)$ (solid).

function $\Phi(t)$ is analytic in the time variable t. If the analytic continuation is done properly, all effects of wave coupling, side wave contributions, etc., are taken into account. In addition, contours which circumvent singularities located at the imaginary axis in a certain distance will lead to a smoother integrand. In particular, the half-residua contributions and the principal value integrals occurring in the limit $\vartheta \to \pi/2$ become much easier to handle.

From the viewpoint of magnetic reconnection there is one peculiarity. Magnetic reconnection produces sources moving along the interface. The result in the complex s plane are poles from the source term (66e) on the imaginary axis. In the limit $\vartheta \to \pi/2$, the contour of integration for real τ runs along the imaginary axis surrounding the poles by semicircles in the fourth quadrant. If a similar integration is done for $\tilde{\zeta}$, the displacement in the lower half space, and the limit $\lim_{z\to 0}(\zeta - \tilde{\zeta})$ is calculated, the contributions from the principal value integrations cancel whereas the contributions from the half residua exactly sum up to the source term $Q(t,x)$. In fact, these poles are the sources of the finite width of the interface of the two media, i.e., the boundary layer produced by reconnection which is now able to act as a sink or source of plasma.

D. Numerical results

The reconnection electric field $E^*(t)$ is chosen as

$$\frac{E^*(t)}{E_0} = 2\left[4t\ \mathrm{e}^{-4t^2}\tanh(2t) + \frac{1-\mathrm{e}^{-4t^2}}{\cosh(2t)}\right], \tag{73}$$

where time has been normalized with respect to the characteristic time of active reconnection T_0. The electric field together with the reconnected flux length $\Phi_0(t)$,

$$\begin{aligned} \frac{\Phi_0(t)}{L_0} &= (1-\mathrm{e}^{-4t^2})\tanh(2t), \\ L_0 &= \frac{cE_0T_0}{B_0} = \frac{cE_0}{\tilde{v}_{A0}B_0}L_A = \varepsilon L_A \end{aligned} \tag{74}$$

[see (42)] is shown in Figure 3. Here, T_0 is some normalizing time unit, L_A the length crossed in time T_0 with speed $\tilde{v}_{A0}$, and L_0 the scale length of the reconnected flux in terms of the background field B_0. For the boundary layer approximation to apply, it is necessary that $L_0 \ll L_A$, i.e., the width of the reconnected magnetic flux tube after time T_0 must be small compared to the distance traveled with characteristic Alfvén speed within T_0.

The magnetic field up to first order is given by

$$\begin{aligned} \mathbf{B}(t,x,y,z) = \mathbf{B}^{(0)} + \varepsilon(&\mathbf{B}^{(0)}\cdot\nabla\boldsymbol{\xi}(t,x,y,z) \\ &- \mathbf{B}^{(0)}\nabla\cdot\boldsymbol{\xi}(t,x,y,z)), \end{aligned} \tag{75}$$

so that, in plane geometry, the components are

$$B_x(t,z,x) = B_x^{(0)}\frac{\partial}{\partial z}(z - \varepsilon\zeta(t,x,z)), \tag{76a}$$

$$B_z(t,z,x) = B_x^{(0)}\frac{\partial}{\partial x}(\varepsilon\zeta(t,x,z)). \tag{76b}$$

Therefore, the magnetic field can be obtained from a flux function ψ,

$$\psi(t,x,z) = B_x^{(0)}(z - \varepsilon\zeta(t,x,z)), \tag{77a}$$

$$B_x(t,z,x) = \frac{\partial}{\partial z}\psi(t,x,z), \tag{77b}$$

$$B_z(t,z,x) = -\frac{\partial}{\partial x}\psi(t,x,z), \tag{77c}$$

and magnetic field lines are just the contours $\psi(t,x,z) = \text{const}$.

In Figure 4, the evolution of the large amplitude waves as well as the linear perturbations in the magnetic field for low plasma beta are shown. By assumption, after time $t=1$, active reconnection along the reconnection line had passed (see Figure 3). During this time interval, a perturbation with speed $\tilde{v}_{A0}$ would cross a distance L_A. These are the units of the x axis. The rotational discontinuity A extends from $x=0$ to $x=(v_{A0}/\tilde{v}_{A0})t = \gamma_A t$, the upper slow shock from $x=0$ to $x=\gamma_S t$, the lower slow shock from $x=0$ to $x=\tilde{\gamma}_S t$, and the contact discontinuity from $x=0$ to $x=(v_2/\tilde{v}_{A0})t$.

For times $t>1$, the single shocks and discontinuities will move as a whole with their appropriate speeds, i.e., v_{A0}, w_S, $\tilde{w}_S$, and v_2 along the x axis. Therefore, the reconnection boundary develops into an elongated structure with a plasma and magnetic flux entry layer at the leading edge, i.e., the lower slow shock S, and another plasma entry but magnetic flux exit layer at the trailing edge, i.e., the upper rotational discontinuity A.

This leads to a remarkable feature of the spontaneous reconnection model. In a first stage, magnetic flux tubes are reconnected inside the diffusion region. In the present context, this amount is proportional to the time-integrated reconnection electric field along the reconnection line, i.e., Φ_0, as defined in (74). This process defines the potential plasma volume (reconnected flux length in the z-direction times the extension of the current sheet in the x direction and times the length of the reconnection line in the y direction) which is going to be heated as well as accelerated by the $\mathbf{j}\times\mathbf{B}$ force when crossing the shock waves. The extension in the

Downloaded¬09¬Apr¬2003¬to¬193.170.90.47.¬Redistribution¬subject¬to¬AIP¬license¬or¬copyright,¬see¬http://ojps.aip.org/pop/popcr.jsp

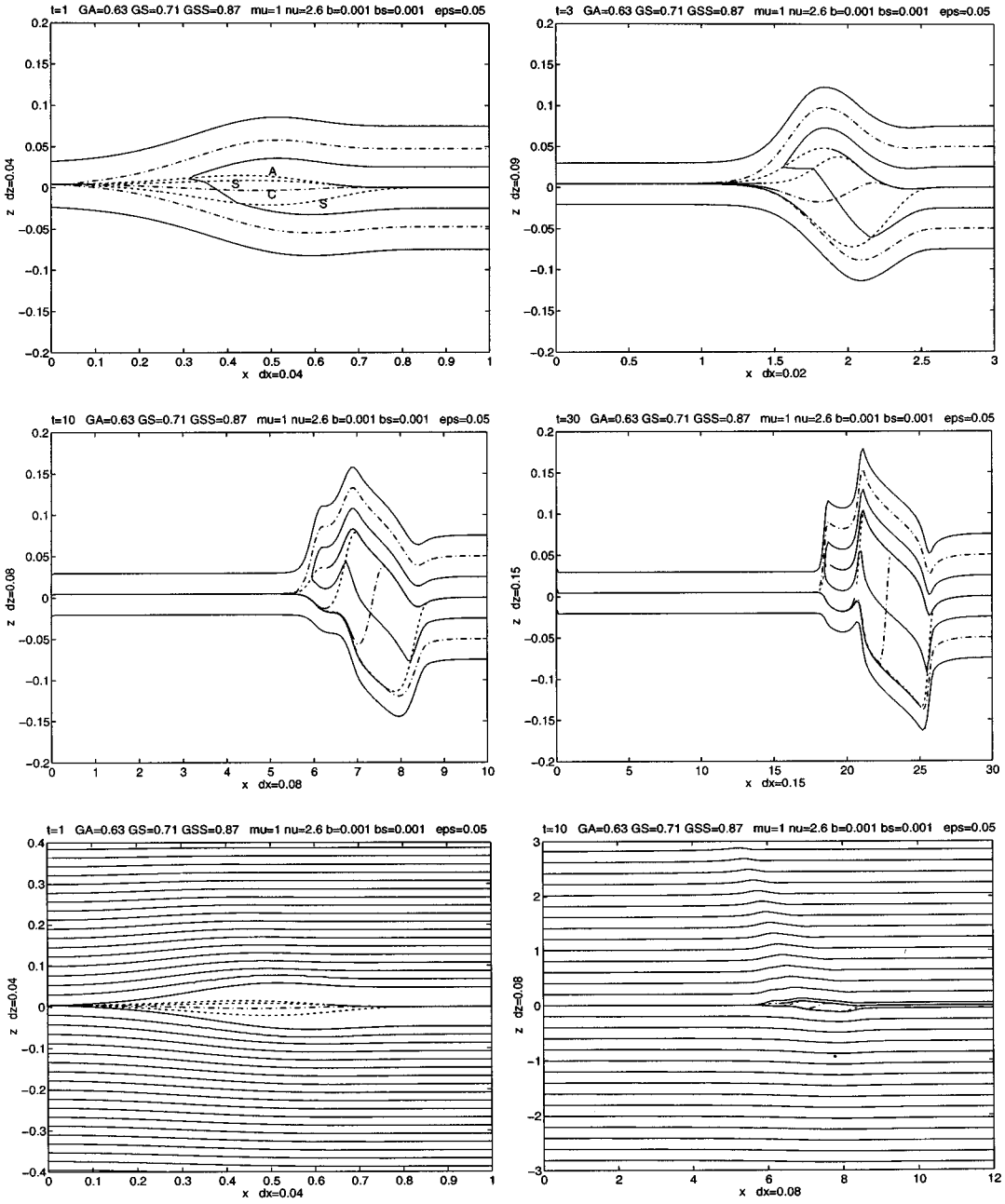

FIG. 4. Evolution of the large wave structures and the first order inflow perturbations for low beta plasma, $\beta=\tilde{\beta}=0.001$. Shown are the rotational discontinuity A (dotted), the slow shocks S (dotted), the contact discontinuity C (dot dashed), the separatrix (dot dashed), a reconnected, and two nearby non-reconnected magnetic field lines. The x and z axes are normalized to L_A and L_0, respectively. The parameters in the top line are time (t), $\gamma_A=v_{A0}/\tilde{v}_{A0}$ (GA), $\gamma_S=w_S/\tilde{v}_{A0}$ (GS), $\tilde{\gamma}_S=\tilde{w}_S/\tilde{v}_{A0}$ (GSS), $\mu=B_0/\tilde{B}_0$ (mu), $\nu=\rho_0/\tilde{\rho}_0$ (nu), $\beta=c_{s0}^2/v_{A0}^2$ (b), $\tilde{\beta}=\tilde{c}_{s0}^2/\tilde{v}_{A0}^2$ (bs), and the reconnection rate $\varepsilon=cE_0/(\tilde{v}_{A0}B_0)$ (eps). The values (dx) and (dz) are the values of numerical resolution of $\zeta(t,x,z)$.

x-direction of the shock waves themselves is proportional to the duration of the reconnection electric field times their wave speed along the current sheet which is approximately the Alfvén speed (one length unit in Figures 4–8). These shock waves start to move along the current sheet carrying with them the history of the reconnection electric field. In such a way, these shocks are able to release further free energy contained in the current sheet in spite of the fact that actual reconnection of magnetic flux tubes had stopped some time before already. Therefore, the efficiency of spontaneous reconnection does not only depend on diffusive processes leading to reconnected flux tubes but also on the geometric extension of the current sheet.

The z axis in Figure 4 is scaled in proportion to the reconnected magnetic flux. It may be noticed that between $t=1$ and $t=30$, the x axis is compressed by a factor of 30 whereas the z axis always has the same scaling. In other words, the structure develops into an extremely elongated structure nearly everywhere closed by tangential discontinuities with short entry layers at the leading and the trailing

Downloaded¬09¬Apr¬2003¬to¬193.170.90.47.¬Redistribution¬subject¬to¬AIP¬license¬or¬copyright,¬see¬http://ojps.aip.org/pop/popcr.jsp

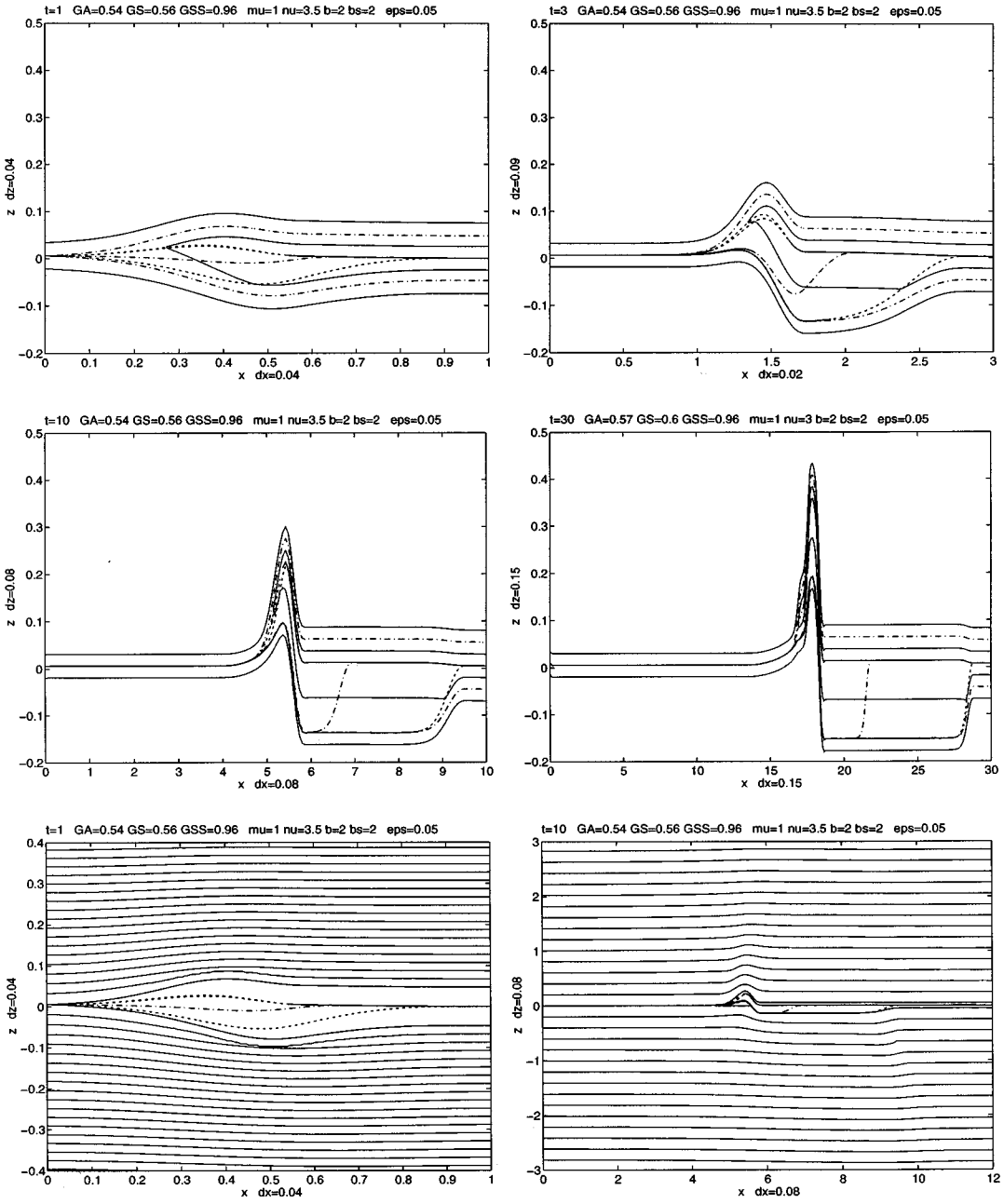

FIG. 5. Same as Figure 4 but for high beta plasma, $\beta=\tilde{\beta}=2$.

edge. This can be better seen in the bottom panel where the perturbations of the magnetic field lines in the inflow regions are shown.

In the low plasma beta limit shown in Figure 4, only the fast wave with nearly isotropic properties contributes to the perturbations in the inflow regions. The wave speed in the upper half plane is by a factor 0.63 lower than in the lower half space. As a result, there are perturbations excited by sources moving with supersonic speed along the x axis. This side wave in the form of a Mach cone can be seen in the right bottom panel of Figure 4 in the half plane $z>0$.

This should be compared to the results shown in Figure 5 for a high beta plasma. In this case, the fast wave can always propagate upstream of the moving sources. As a result, the side wave is absent and also the more or less linear decrease of the separatrix between rotational discontinuity and leading slow shock is absent. It can also be seen that in the limit of high plasma beta, the rotational discontinuity and upper slow shock merge together. This is to be expected because the slow and the Alfvén phase speeds become identical in this limit.

It is interesting, to compare the low and high beta limit for symmetric conditions in the inflow regions. The results are shown in Figure 6. In this case, the rotational discontinuity and the slow shock merge to a single shock of switch-off type. This is the strongest form of a slow shock where the upstream tangential magnetic field component is 'switched-off' completely in transition to the downstream side. Also, in

Downloaded¬09¬Apr¬2003¬to¬193.170.90.47.¬Redistribution¬subject¬to¬AIP¬license¬or¬copyright,¬see¬http://ojps.aip.org/pop/popcr.jsp

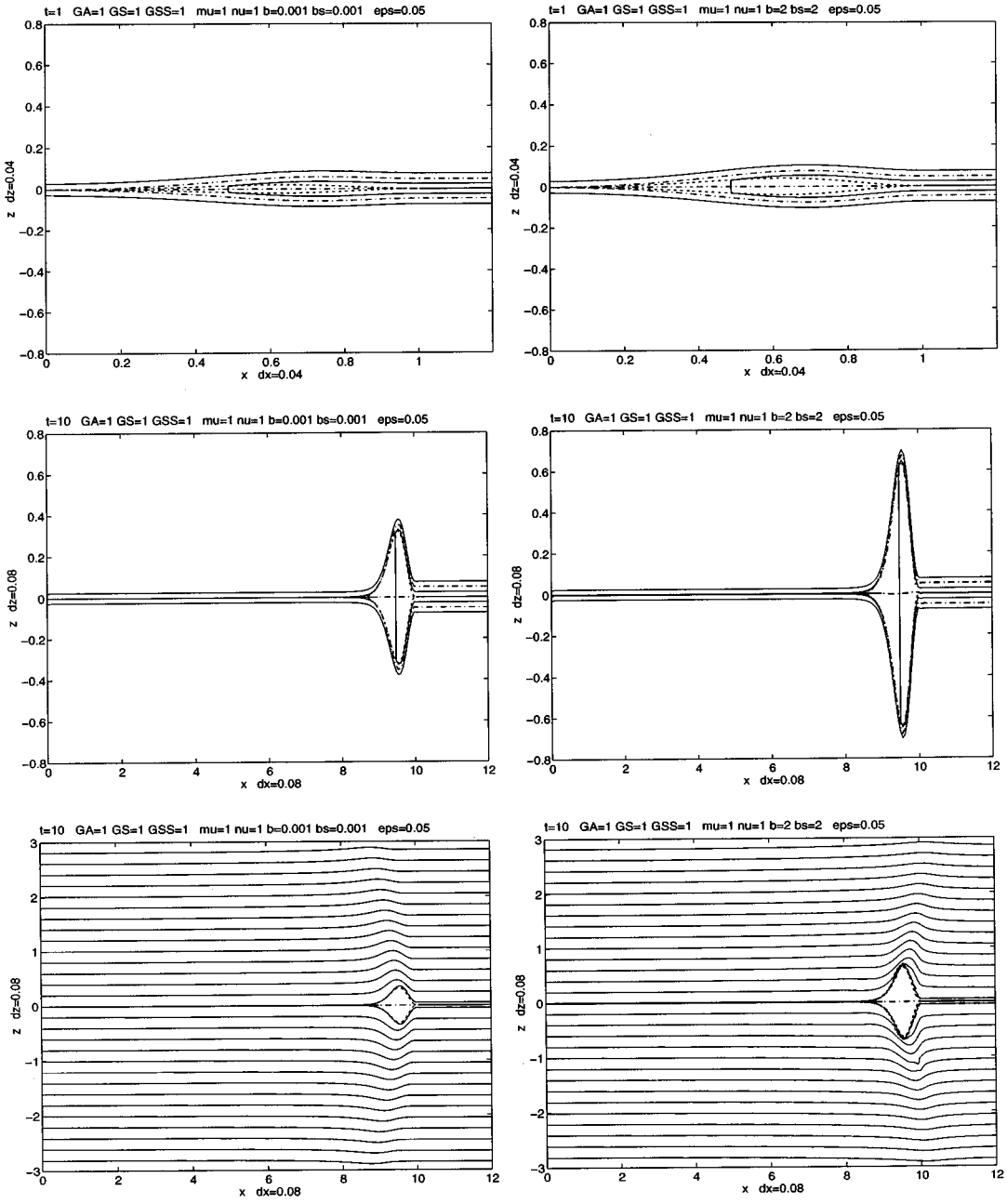

FIG. 6. Evolution of discontinuities and inflow perturbations for symmetric conditions in the inflow regions. The left panel shows the results in the low beta limit, the right panel shows the same in the high beta limit.

the low beta case the plasma is more compressed across the slow shocks than in the high beta case. Therefore, mass conservation requires that the region of field reversal inside the separatrix is larger in the high beta limit. This is true for all cases as can be observed in the different figures. In the bottom panel on the left, $\beta=0.001$, one can see clearly the wave front at $r=v_{A0}t$, whereas on the right, $\beta=2$, the fast wave modifies the conditions already upstream of the source moving in both cases with speed v_{A0} along the x axis.

An example for highly asymmetric conditions is shown in Figure 7. The plasma in the upper half space is practically incompressible, whereas the plasma in the lower half space is highly compressible. As a result, the incompressible precursor waves produce a remarkable perturbation into the lower half space at the leading edge of the field reversal region.

Another interesting case, namely the generation of a surface wave mode is shown in Figure 8. In this case, in addition to the poles created by the source function $\bar{Q}$ in (59b), the denominator function $\bar{L}+\tilde{L}$ also has a zero. Such a zero only occurs for very specific background conditions. For a low beta plasma it may look like that in Figure 8 corresponding to a perturbation moving behind all other structures. In the limit of a high beta plasma (incompressible limit), such a pole will appear in the velocity range between the upper and the lower Alfvén speed. In the exact incompressible limit, only the half-residua from the poles of the integrand contribute and the integrals can be evaluated explicitly. The princi-

Downloaded¬09¬Apr¬2003¬to¬193.170.90.47.¬Redistribution¬subject¬to¬AIP¬license¬or¬copyright,¬see¬http://ojps.aip.org/pop/popcr.jsp

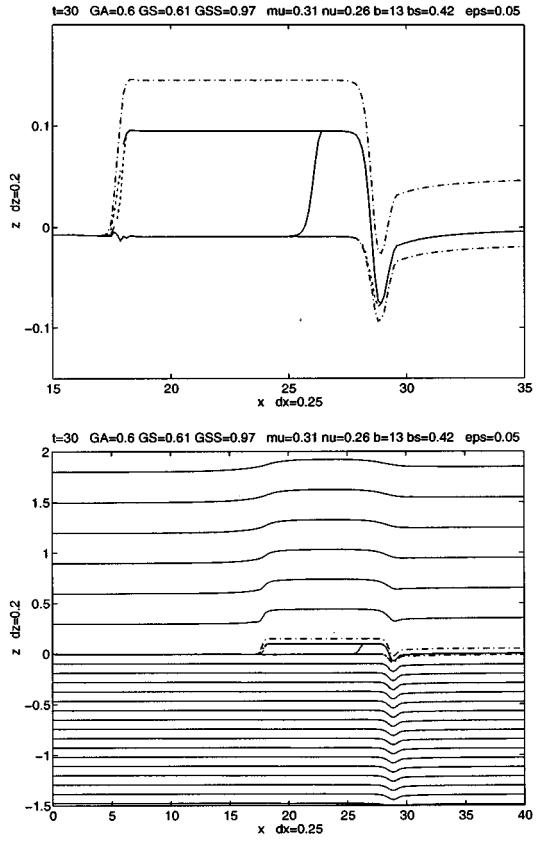

FIG. 7. Structure of the reconnected flux tube (upper panel) and the corresponding inflow perturbations (lower panel) for highly asymmetric conditions, $B_0/\tilde{B}_0=0.31$, $\rho_0/\tilde{\rho}_0=0.26$ (upper to lower half plane values). Reconnection at $x=0$ had stopped approximately 30 time units ago. In the upper half plane the sound speed exceeds the Alfvén speed, $c_s/v_A=3.6$, whereas in the lower half plane the sound speed is less than the Alfvén speed, $c_s/v_A=0.65$.

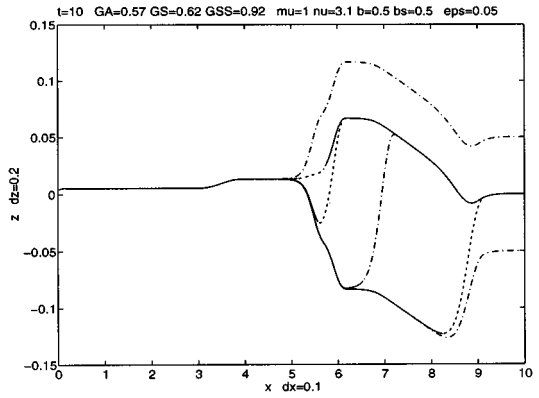

FIG. 8. Appearance of a surface mode between $3\leqslant x\leqslant 4$ which moves with a speed slower than both the upper and the lower Alfvén speed.

pal value contributions describe wave coupling effects which are absent in the incompressible limit but also vanish in the long-time compressible limit.

VI. CONCLUSIONS

In the present paper the process of magnetic reconnection is comprehensively studied within the framework of ideal magnetohydrodynamic theory. It is assumed that the non-ideal process of 'cutting and reconnecting' the magnetic field lines is, on the ideal MHD scale, extremely localized and therefore all non-ideal processes can be lumped together and described by a given time dependent reconnection electric field tangential to a given reconnection line on an ideal current surface with magnetic shear, i.e., a tangential discontinuity.

This reconnection electric field, generated locally by non-ideal processes, induces shear waves, i.e., Alfvén and slow wave modes, which propagate the tangential electric field itself along the current sheet (tangential discontinuity). Connected with the tangential electric field is a normal magnetic field component. Along this field component, Alfvén and slow waves can redistribute the initial current. The solution of this problem for an arbitrary tangential discontinuity, also known as generalized Riemannian problem, has been solved earlier already and is briefly reviewed.

On the basis of this non-linear solution, the ideal compressible MHD system is linearized. In addition, Alfvén and slow waves propagate predominately along the unperturbed magnetic field. This produces very thin elongated structures and a boundary layer approximation can be used. A central result of the present paper is the complete determination of mass and magnetic flux into and out of this boundary layer.

The perturbations in the inflow regions are determined from an exact solution of the compressible MHD system. Boundary conditions are total pressure balance across the boundary layer and zero perturbations at large distances. The condition for zero perturbations at large distances corresponds to 'spontaneous reconnection', i.e., the source is a local reconnection electric field. The analysis presented could easily be extended to the case of 'driven reconnection', i.e., a given inflow of plasma and magnetic flux at large distances (global electric field), or a combination of both. The problem is equivalent to the linear evolution of perturbations in two half spaces with different anisotropic multimode wave properties coupled by total pressure balance at the interface. Magnetic reconnection widens this interface into a boundary layer which acts now as a source and sink of plasma and magnetic flux. The appropriate self-consistent source term for a given reconnection electric field is determined in Laplace Fourier space.

Finally it is shown, how, in plane geometry, the exact solution can be written as a convolution with an appropriate Green's function. The properties of this Green's function which satisfy the total pressure balance condition at the interface of the two half planes, the correct boundary conditions at infinity, causality, and the anisotropic nature and coupling of all three MHD modes in each half plane are discussed in the plane of complex phase velocities.

The effects of changing the plasma beta, i.e., plasma pressure versus magnetic pressure, are discussed. It is shown how a side wave is generated in a low beta plasma as the result of a supersonic source moving along the interface and how this is modified in a high beta plasma when the source becomes subsonic with respect to the fast wave speed.

Explicit numerical results for compressible reconnection

Downloaded¬09¬Apr¬2003¬to¬193.170.90.47.¬Redistribution¬subject¬to¬AIP¬license¬or¬copyright,¬see¬http://ojps.aip.org/pop/popcr.jsp

of magnetic field lines are given for asymmetric and symmetric conditions in the inflow regions. The reconnection induced perturbations move like a flat deformable object, the field reversal region, along the current sheet. In the course of time, the field reversal region becomes an extremely elongated object bounded nearly everywhere by tangential discontinuities with the exception of plasma and magnetic flux entry layers at the leading and the trailing edge. The mass inside the reconnected flux tubes, i.e., inside the separatrix, is continuously collected into this field reversal region. By this effect, the spontaneous reconnection model discussed becomes a very effective energy converter. Plasma is accelerated and heated not only during the active reconnection period which might be very short but during all the time the field reversal region is moving along the current sheet.

ACKNOWLEDGMENTS

V. S. S. was partially supported by the Russian Foundation for Fundamental Research under Grant No. 93-05-17268a and also acknowledges the financial support from the Technical University Graz and the hospitality of the Institut für Theoretische Physik during a scientific visit to Graz.

[1]V. C. A. Ferraro, J. Geophys. Res. **57**, 15 (1952).
[2]V. C. A. Ferraro, Ann. Geophys. **11**, 284 (1955).
[3]J. W. Dungey, *Cosmic Electrodynamics* (Cambridge University Press, London, 1985), p. 183.
[4]M. N. Rosenbluth, in *Plasma Physics and Thermonuclear Research*, edited by C. L. Longmire, J. L. Tuck, and W. B. Thompson (Pergamon, Oxford, 1963), Vol. 2, p. 271.
[5]P. A. Sweet, in *Electromagnetic Phenomena in Cosmical Physics*, edited by B. Lehnert (Cambridge University Press, London, 1958).
[6]E. Parker, Astrophys. J. Suppl. Ser. **8**, 177 (1963).
[7]H. E. Petschek, in *AAS-NASA Symposium of the Physics of Solar Flares, NASA-SP 50*, edited by W. N. Hess (National Aeronautics and Space Administration, Washington, DC, 1964), pp. 425–439.
[8]H. E. Petschek, in *The Solar Wind, JPL Technical Report No. 32-630*, edited by R. J. Mackin, Jr. and M. Neugebauer (California Institute of Technology Press, Pasadena, 1966), pp. 257–273.
[9]H. E. Petschek, in *Physics of the Magnetopause*, Geophysical Monograph 90, edited by P. Song, B. U. O. Sonnerup, and M. F. Thomsen (American Geophysical Union, Washington, DC, 1995), pp. 21–28.
[10]R. H. Levy, H. E. Petschek, and G. L. Siscoe, AIAA J. **2**, 2065 (1964).
[11]H. E. Petschek and R. M. Thorne, Astrophys. J. **174**, 1157 (1967).
[12]M. F. Heyn, H. K. Biernat, V. S. Semenov, and I. V. Kubyshkin, J. Geophys. Res. **90**, 1781 (1985).
[13]M. F. Heyn, H. K. Biernat, R. P. Rijnbeek, and V. S. Semenov, J. Plasma Phys. **40**, 235 (1988).
[14]Y. Lin and L. C. Lee, Space Sci. Rev. **65**, 59 (1993).
[15]C.-K. Yang and B. U. O. Sonnerup, J. Geophys. Res. **82**, 699 (1977).
[16]A. M. Soward and E. R. Priest, J. Plasma Phys. **28**, 335 (1982).
[17]V. S. Semenov, I. V. Kubyshkin, and M. F. Heyn, J. Plasma Phys. **30**, 303 (1983).
[18]V. S. Semenov, I. V. Kubyshkin, M. F. Heyn, and H. K. Biernat, J. Plasma Phys. **30**, 321 (1983).
[19]V. S. Semenov, M. F. Heyn, and I. V. Kubyshkin, Sov. Astron. **27**, 660 (1983).
[20]M. F. Heyn, H. K. Biernat, and V. S. Semenov, Adv. Space Res. **6**, 115 (1986).
[21]H. K. Biernat, M. F. Heyn, and V. S. Semenov, J. Geophys. Res. **92**, 3392 (1987).
[22]V. S. Semenov and A. A. Shmalts, Geomagn. Aeron. **28**, 483 (1988).
[23]V. S. Semenov, I. V. Kubyshkin, V. V. Lebedeva, M. V. Sidneva, H. K. Biernat, M. F. Heyn, B. P. Besser, and R. P. Rijnbeek, J. Geophys. Res. **97**, 4251 (1992).
[24]M. F. Heyn, in *Solar Wind-Magnetosphere Interactions*, edited by M. F. Heyn, H. K. Biernat, V. S. Semenov, and R. P. Rijnbeek (Österreichische Akademie der Wissenschaften, Vienna, 1992), pp. 85–112.
[25]M. F. Heyn, in *Physics of the Magnetopause*, Geophysical Monograph 90, edited by P. Song and B. U. O. Sonnerup (American Geophysical Union, Washington, DC, 1995), pp. 189–195.
[26]M. Scholer, J. Geophys. Res. **94**, 8805 (1989).
[27]M. Ugai, Phys. Plasmas **1**, 2853 (1994).
[28]M. Ugai, Phys. Plasmas **2**, 388 (1995).
[29]H. P. Furth, J. Killeen, and M. N. Rosenbluth, Phys. Fluids **6**, 459 (1963).
[30]M. Ottaviani and F. Porcelli, Phys. Plasmas **2**, 4104 (1995).
[31]H. Lamb, Philos. Trans. R. Soc. London Ser. A **203**, 1 (1904).
[32]A. I. Akhiezer, I. A. Akhiezer, R. V. Polovin, A. G. Sitenko, and K. N. Stepanov, *Plasma Electrodynamics* (Pergamon, Oxford, 1975).
[33]H. Weitzner, in *Basic Plasma Physics I*, edited by A. A. Galeev and R. N. Sudan (North-Holland, Amsterdam, 1983), pp. 201–242.
[34]A. Jeffrey and T. Tanuiti, *Non-Linear Wave Propagation* (Academic, New York, 1964).
[35]D. G. Wentzel, Astrophys. J. **227**, 319 (1979).
[36]A. K. Sen, Phys. Fluids **7**, 1293 (1964).
[37]J. A. Hudson, *The Excitation and Propagation of Elastic Waves* (Cambridge University Press, London, 1980).
[38]T. Rikitake, R. Sato, and Y. Hagiwara, *Applied Mathematics for Earth Scientists* (Terra Scientific, Tokyo, 1987).

Downloaded¬09¬Apr¬2003¬to¬193.170.90.47.¬Redistribution¬subject¬to¬AIP¬license¬or¬copyright,¬see¬http://ojps.aip.org/pop/popcr.jsp